The University of Western Australia

School of Electrical, Electronic and Computer Engineering

The REV Project
THE UNIVERSITY OF WESTERN AUSTRALIA

Development of a Navigation Control System for an Autonomous Formula SAE-Electric Race Car

Thomas H. Drage

20510505

Final Year Project Thesis submitted for the degree of Bachelor of Engineering.

Submitted 1st November 2013

Supervisor: Professor Dr. Thomas Bräunl

Abstract

Figure 1: Autonomous Formula SAE-Electric Car

This dissertation describes the development of a high level control system for an autonomous Formula SAE race car featuring fusion of a 6-DOF IMU, a consumer grade GPS and an automotive LIDAR. Formula SAE is a long-running annual competition organised by the Society of Automotive Engineers which has recently seen the introduction of the new class SAE-Electric. The car discussed in this dissertation features electric motors driving each of the two rear wheels via independent controllers and has full drive-by-wire control of the throttle, steering and (hydraulic) braking system. Whilst autonomous driving is outside the scope of the Formula-SAE competition, it has been the subject of significant research interest over the last several decades. It is intended that the Autonomous SAE car developed in this project will provide UWA with a platform for research into driverless performance cars.

This project consists of the design and implementation of a navigation control system which uses a Linux PC to interface with a range of sensors as well as the drive-by-wire system, safety systems and a base station. The navigation control system is implemented as a multi-threaded C++ program featuring asynchronous communication with hardware outputs, sensor inputs and user interfaces. The Autonomous SAE Car can drive following a map consisting of “waypoints” and “fence posts” which are recorded by either driving the course manually or through a GoogleMaps based web interface. Mapped driving is augmented by the use of a LIDAR scanner for detection of obstacles including road edges for which a novel algorithm is presented. GPS is used as the primary navigation aid; however sensor fusion algorithms have been implemented in order to improve upon the measurement of the cars position and orientation through the use of a 6-DOF Inertial Measurement Unit.

Attention to safety is essential in such a project as the car weighs in excess of 250kg and is capable of driving at a speed of 80km/h. Safety systems are implemented as part of the navigation controller as well as through independent hardware. Facilities for remote intervention and emergency stopping are provided through a wireless link to the base station as well as through hard-wired systems on the car itself.

Measurements derived from autonomous test driving as well as the sensor fusion and road-edge detection algorithms are presented as well as an overview of the future potential of the platform as a research tool.

Acknowledgements

I would like to thank the following people for their assistance in this project:

Prof. Thomas Bräunl for his guidance, advice and commitment to the REV Project.

The REV Autonomous SAE Team for their invaluable assistance and camaraderie.

My friends and family for their support and encouragement over the course of this year.

John Cooper and the team at EV Works who have provided us with advice and assistance with manufacturing parts.

Galaxy Resources, Altronics and Swan Energy for their generous donations to the REV Project.

Western Power for the support of their undergraduate scholarship programme.

See Appendix A for acknowledgement of the authors of software libraries used in this project.

Nomenclature

AJAX	Asynchronous JavaScript and XML
API	Application Programming Interface
ARM	Advanced/Acorn RISC (Reduced Instruction Set Computer) Machine
NO	Normally Open
NC	Normally Closed
BMS	Battery Management System
COM	(Microsoft) Component Object Model
FIFO	First In, First Out
GPS	Global Positioning System
HTML	Hypertext Markup Language
HTTP	Hypertext Transfer Protocol
IC	Integrated Circuit
IO	Input/Output
INS	Inertial Navigation System
IMU	Inertial Measurement Unit
JSON	JavaScript Object Notation
LIDAR	Light Detection and Ranging
NMEA	National Marine Electronics Association
POSIX	Portable Operating System Interface
RAM	Random Access Memory
TTL	Transistor-Transistor Logic
UART	Universal Asynchronous Receiver/Transmitter
USB	Universal Serial Bus
UI	User Interface
SAE	Society of Automotive Engineers
SLA	Sealed Lead Acid
WDT	Watchdog Timer
Wifi	Wireless Local Area Network (e.g. IEEE 802.11)

Table of Contents

Abstract....i
Acknowledgements....iii
Nomenclature....iv
1 Introduction and Background....1
1.1 Introduction....1
1.2 Motivation....2
2 Literature Review....3
3 System Design....5
3.1 Overview and Requirements....5
3.2 Hardware Framework....6
3.3 Communication and Integration....8
3.4 Software Framework....9
Navigation Control Program....9
Base Station Hardware IO Software....12
Web Interface....13
4 Sensor Selection and Integration....14
4.1 Overview....14
4.2 Position and Orientation....15
Global Positioning System....15
Inertial Measurement Unit....17
Sensor Fusion....18
Vehicle Heading....19
Positioning....22
4.3 Physical Environment....24
IBEO LIDAR....24
Road Edge Detection....25
Mapping of Obstacles....31
5 Instrumentation and Control....33
5.1 Mapping....33
Geodesy....33
Implementation....34
5.2 Trajectory Calculation and Driving....34
Overview....34
Heading....35
Simple Steering Algorithm....35
Improved Steering Algorithm....37
Speed....38
5.3 User Interfaces....39
Base Station Driven....40
Base Station Hardware Interface....40
Web Interface....40
Self Contained Operation....42
6 Safety....43
6.1 Requirements and Design....43
Risk Assessment....43
System Design....44

6.2 Integrated Safety Features....45
6.3 Hardware Safety Supervisor....47
Hardware....47
Software State Machine....50
7 Results....52
7.1 Position & Heading....52
7.2 Road Edge Detection....54
Scenario 1 – Curb Detection on an Asphalt Road....54
Scenario 2 – Grass Edge Detection on a Paved Road....56
Scenario 3 – Curb Detection with Lateral Motion....58
Performance of Edge Finding Modes....59
7.3 Autonomous Driving....60
8 Conclusion and Future Work....63
Conclusion....63
Future Work....64
References....65
Appendices....71
Appendix A – Acknowledgement of Software Licensors....71
Appendix B – Drive-by-wire Command Set....72
Appendix C – Base Emergency Stop Wiring Diagram....73
Appendix D – Web Interface....74
Appendix E – Risk Register....76
Appendix F – Hardware Safety Supervisor Circuit....77
Appendix G – Safety Supervisor State Diagram....78
Appendix H – Safety Supervisor State Outputs....79

1 Introduction and Background

1.1 Introduction

The automotive industry has undergone a revolution over the last decade with technologies such as driver assistance systems and hybrid/electric drive systems developed in the fields of robotics and electronics making their way into an industry dominated by fossil fuelled vehicles with limited intelligence. This revolution however, is far from over with electric vehicles still yet to make significant headway in the market and robotic functionality limited to auxiliary systems used to assist the driver and compensate for their weaknesses. Automotive racing has seen the development of many advanced technologies throughout the history of vehicular transport, however, there has been little cross-over with robotic technologies as the focus of most competitions is in the optimisation of technology, driver skill and team organisation.

Formula SAE [1] is a long-running annual competition organised by the Society of Automotive Engineers with competition events in the U.S., Europe, Brazil, Japan and Australia. In former years Formula SAE has been a design competition only for petrol cars, but recently the new class SAE-Electric has been introduced. In addition to two road-registered electric vehicles (EVs), a Hyundai Getz and a Lotus Elise, UWA's Renewable Energy Vehicle Project (REV) has built two electric SAE cars. The vehicle discussed in this dissertation features electric motors driving each of the two rear wheels via independent controllers and has full drive-by-wire control implemented by Jordan Kalinowski in a parallel project. A system has been implemented featuring electronic control of the vehicles throttle, actuation of the hydraulic brakes and motorised steering.

Figure 2: Formula SAE-Electric Frame

This is outside the scope of the SAE competition which neither allows drive-by-wire nor autonomous drive systems, however, the Autonomous SAE car project will provides UWA with a platform for research into driverless cars. In particular, this project builds past research conducted at UWA in which the REV group have implemented brake-by-wire and steer-by-wire for a driver-assistance system on a BMW X5 [2]. The total automation and scope for modification provided by the Autonomous SAE car give rise to research possibilities including, but not limited to, automated performance driving, automated mapping and intelligent driving.

This dissertation describes the development of a map based autonomous driving system and incorporates development of systems and technologies essential to any autonomous driving application that may be developed in the future using this vehicle. Particular focus is given to the hardware and software frameworks for implementation of this functionality, the integration of an array of relevant sensors, LIDAR based road-edge detection and trajectory computation and control. Safety systems have been considered as an integral part of the car's functionality and a comprehensive range of controls have been developed in conjunction with Jordan Kalinowski.

1.2 Motivation

The development of the Autonomous SAE Car is primarily motivated by the great potential for research into control systems, information processing algorithms and sensory techniques that are made possible by creation of this vehicle as a research platform. This dissertation describes the creation of such a platform, as well as a small proportion of the possible techniques that are able to be developed and tested to further the field of mobile robotics. In particular, as the Autonomous SAE Car is a race car by nature, research is possible within the rather underdeveloped field of autonomous performance driving. Traditional automobile racing is considered to be at the forefront of technology and has seen significant technological advances which have filtered down to more mundane transportation systems and it is therefore expected that the same will apply in the field of autonomous driving.

Research into autonomous driving has significant commercial potential as it represents the next revolution in the efficiency of almost all transportation systems. Autonomous trains are already fairly commonplace, particularly in niche operations such as mass rapid transport systems [3] and mining [4] and have obvious advantages in terms of their operating costs and scheduling. Automated truck convoying has also received significant commercial interest for similar reasons [5]. It is therefore evident that technologies developed at UWA utilising the Autonomous SAE Car have significant potential for real-world application in the near future.

2 Literature Review

Research into autonomous vehicles began in the 1980s with projects such as the EUREKA Prometheus Project in Europe and the United States' Autonomous Land Vehicle Project [6]. The DARPA Grand Challenges [7][8] in 2004 and 2005 saw teams of autonomous vehicles competing to navigate a desert environment whilst the 2007 Urban Challenge [9][10][11] required navigation of a road based course and adherence to traffic protocols. In Europe, the VisLab Intercontinental Autonomous Challenge in 2010 [12] required an autonomous drive following a leader car from Italy to China. These competitions saw massive development of the field, with advanced technologies already becoming available for automotive use. Autonomous driving technology is evolving rapidly and is well on its way to finding commercial use in years to come. Google recently revealed that their fleet of autonomous cars had travelled 140,000 miles on US public roads without human intervention [13]. Locally, Rio Tinto plans to have 150 autonomous trucks supplied by Komatsu working in their Pilbara mining operations by 2015 [14].

Figure 3: Stanley - the winner of the 2005 DARPA Grand Challenge. Source: [7]

Figure 4: Komatsu autonomous dump trucks. Source: [15]

Over the last decade driver assistance systems have gradually become standard in new cars though most current offerings are of limited sophistication. Adaptive cruise control utilising a laser sensor was first offered by Toyota in 1998, with systems designed to pre-empt potential crashes becoming available on Mercedes-Benz models in 2002 [16]. Since then more advanced camera-based systems such as lane-keeping assistance systems and driver drowsiness detection have become commonplace [16]. Most systems are minimally invasive and have are designed simply to augment the shortcomings of the human driver. The future of this technology holds significant promise for improving road safety and is exemplified by research at Daimler, which offers novel functionality such as the detection of dangerous situations in roundabouts [17].

Detailed research on control systems for autonomous driving have also been carried out at Stanford [18] as well as at the University of Parma [19] and through a collaboration of Spanish universities [20]. At UWA Lochlan Brown has conducted research into stability control using the same car and has provided evidence that computer control of only the throttle has resulted in significant advantages in increasing the vehicles stability [21]. A substantial body of work exists concerning sensory techniques for use in autonomous vehicles including sensors such as GPS on both road vehicles [22] and in agricultural applications [23] and LIDAR [24] [25] [26].

Recently technologies have matured and research into the potential of autonomous cars in racing has begun, with projects such as Stanford University's autonomous Audi TTS, which has been able to perform as well as seasoned racing drivers [27]. This project is of particular interest as its aims in using electronic control systems to drive “at the limits” of the car's mechanical abilities are similar to our project. A sophisticated suite of navigation sensors are used and have seen the car drive complex, long (20km) race courses [22].

Figure 5: Stanford's GPS driven race car "Shelley".
Source: [22]

3 System Design

3.1 Overview and Requirements

The scope of the control system required for this project consists of everything from a user-interface to physical actuation of the car's brake pedal and consists of a significant body of work. It was decided that the Autonomous SAE Car control system would consist of two segments – a “low level system” which handles physical outputs (e.g. signal to the motor controllers, operation of the brake servomotor and steering control system) and the “high level system” which encompasses processing sensor data, communication with the human operator, calculation of control parameters and the subsequent instruction of the low level system. This approach allowed the project to be divided amongst the REV Autonomous SAE Project team and the modularity of the systems provides benefits in terms of testing as well as future expansion.

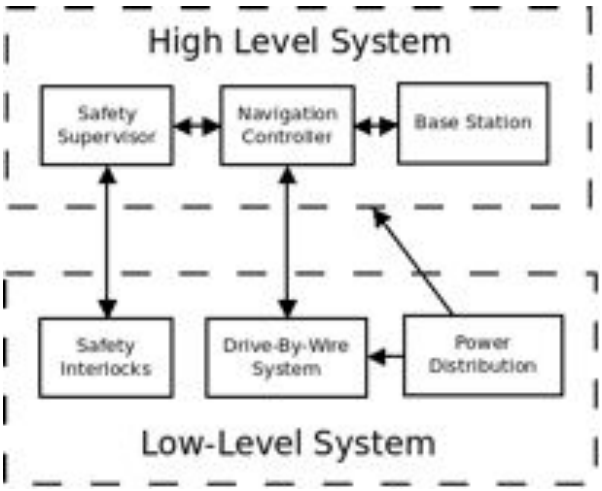

Figure 6: Major components of the Autonomous SAE car control systems.

The high level control system must allow the Autonomous SAE car to drive a pre-recorded map in a manner which is efficient and accurate. Sensor data must be used so that the car can reliably stay on a roadway and for the detection of obstacles in the car's path. Functionality must be provided for editing and recording of maps as well as controlling the system in a simple and convenient fashion. The system must have on-car processing but allow for remote interaction and include the necessary functions to ensure that testing and operation of the vehicle can be carried out safely.

The requirements of the high level control system discussed in this thesis can further be broken up into four distinct sections; the user interface, the sensor systems, the navigation algorithms and finally the safety functionality implemented throughout the system. In meeting the

requirements of these aspects of the project, a framework of hardware and software was created as the basis for implementing functionality. This framework must thus be able to handle a significant amount of data processing, interface with a variety of sensors, provide means for interconnection with subsystems and also provide sufficient scope for expansion in future projects.

3.2 Hardware Framework

Driver assistance systems such as that implemented in 2011 on the UWA BMW X5 vehicle [28] are commonly centred around relatively powerful micro-controllers (e.g. the Eyebot M6) and exist as isolated embedded systems. However, whilst such systems are compact and robust, they are not ideal for the development of a platform for experimentation in which significant future expansion is expected. A survey of other autonomous vehicle projects [7][9][12][20][22][23][29] showed that standard x86 architecture PCs are commonly used in such applications, with benefits including a large amount of processing power and ease of integration with off-the-shelf peripherals. However, in this instance, the car does not possess the space for a full sized computer as well as a constraint existing in the amount of power able to be drawn from the DC-DC converter located in the low-level system.

Two readily available alternatives were investigated, the first being the Raspberry Pi which is a miniature embedded computer featuring a 700MHz ARM processor, 512 MB of RAM and a Secure Digital (SD) card for storage. Secondly, a 2go Netbook based on an Intel Atom processor with 1GB of RAM and a flash SSD was considered and ultimately used throughout the majority of testing and design of this vehicle. The 2go is particularly small and robust, has a battery which allows the system to keep running independently of the DC-DC converter, has built-in Wifi and more importantly has a touchscreen display, trackpad and keyboard. This additional functionality proved extremely useful during testing as the computer is able to be interacted with easily, allowing code changes on the fly and testing independent of the car's systems. More recently, Calvin Yapp has worked on developing an interface for the Raspberry Pi allowing for self-contained operation of the entire system. Both the 2go Netbook and Raspberry Pi run a Linux operating system (Lubuntu and Raspbian respectively) which has built-in drivers for all of the hardware interfaces used in this project and provides a POSIX compliant development environment, assisting in code portability.

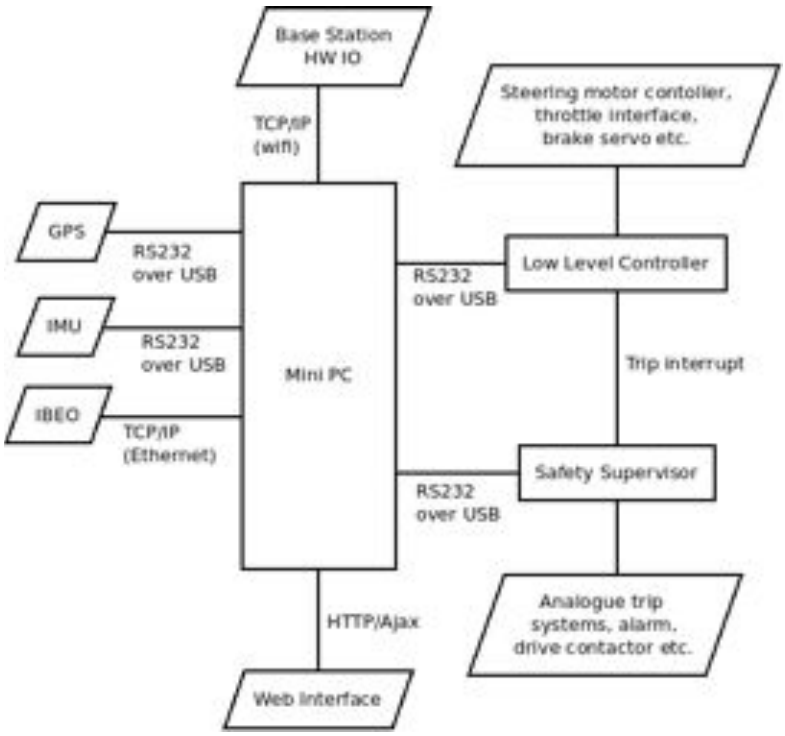

Figure 7: System overview

By using a standard computer system, interconnection of peripherals is simplified significantly as specific interfacing hardware is not required (see Figure 7). An Ethernet switch located in the car provides connectivity for the IBEO LIDAR and Wifi link to the base station with all other sensors and outputs communicating using USB interfaces which are easily duplicated by means of a small USB hub. The 2go Netbook used in this project was conveniently able to be powered from 12V derived from the low-level systems DC-DC converter as was the IBEO LIDAR unit. The Ethernet switch purchased required a 5V DC and so a small sealed 5W DC-DC was obtained to step-down the voltage.

The base station takes the form of a normal Windows laptop with a large physical emergency stop button connected and powered via a USB port. The wireless connection to the car is provided by means of a pair of Ubiquiti PicoStation transceivers which implement a standard IEEE 802.11g Wifi system. The unit located on the car is configured as an access point and powered from the 12V system via a Power Over Ethernet injector, while the PicoStation used as a client at the base station is powered via a 12V SLA battery. The PicoStation's offer 1W of output power and a claimed range of 500m outdoors which is ideal for this application.

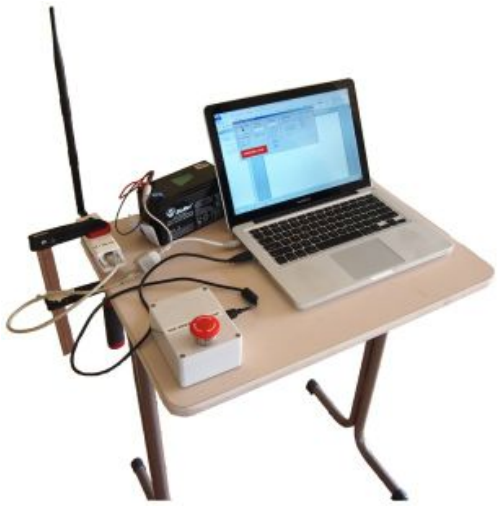

Figure 8: Base station setup.

3.3 Communication and Integration

A variety of different sensors have been used with a number of different interfaces and communication protocols (see Table 1, below) have been implemented in this project. In particular, they fall into two categories – those which use TCP/IP over Ethernet and those which use serial port emulation over USB. The use of TCP/IP is ubiquitous on modern computer networks and is ideal for interconnection of physically separated computer systems and has hence been used to allow easy communication with the car from the base station. The IBEO Lux sensor offers both an RS-232 (serial) and Ethernet interface, however the Ethernet interface has been used as it is more robust [2], faster and in this instance easier to implement (an RS-232 interface is not required).

Serial data transfer is extremely simple to implement and featured on almost all embedded controllers and as such is found in the DATAQ IO module, GPS and IMU units and was implemented for the drive-by-wire controller and hardware safety supervisor. However, due to the lack of hardware serial ports on modern computers many devices utilise a serial-USB bridge which presents as a serial port on the host operating system allowing compatibility with existing software. All of the USB devices in this project utilise such an interface, however in many cases manufacturer provided libraries are still required in order to decode the data sent over the serial bus.

Device/Interface	*Physical Medium*	*Transport*	*Protocol*	*Implementation*
Base Station	Wifi (802.11g)	TCP/IP	ASCII Commands (see section 6.4)	Custom
DATAQ IO Module	USB	Proprietary Serial Port Emulation	Proprietary	DATAQ COM API
GPS Receiver	USB	Serial Port Emulation	NMEA 0183	gpsd Library
IBEO LIDAR	Ethernet	TCP/IP	Proprietary	Custom (Tim Black)
IMU	USB	Serial Port Emulation	Proprietary (CMT)	CMT API
Drive-by-wire Controller	USB	Serial Port Emulation	ASCII Commands (see Appendix B)	Custom
Safety Supervisor	USB	Serial Port Emulation	ASCII Commands (see section 9.3)	Custom
Web Interface	Wifi (802.11g)	TCP/IP	HTTP – JSON/HTML	lighttpd and Perl CGI

Table 1: Communication protocols used in this project.

3.4 Software Framework

Navigation Control Program

The navigation control program itself is implemented in C++, is multi-threaded and handles IO operations asynchronously. This approach was chosen due to the need to reliably communicate across a number of interfaces and for the ability to easily modularise the system. Code is grouped into classes with the system coordinated by the master Control class which acts to initialise the system, provides output of information data, handles map operations and performs trajectory calculations. Each communication channel with the outside systems is implemented inside a separate class which creates a new thread upon its instantiation. These threads handle IO with the outside systems and actions based upon messages received. Classes also exist to handle fusion of the IMU and GPS data and perform logging operations. A number of third party C/C++ libraries have been used in this project, particularly for communication with hardware devices and performing common operations (see Appendix A for a full listing).

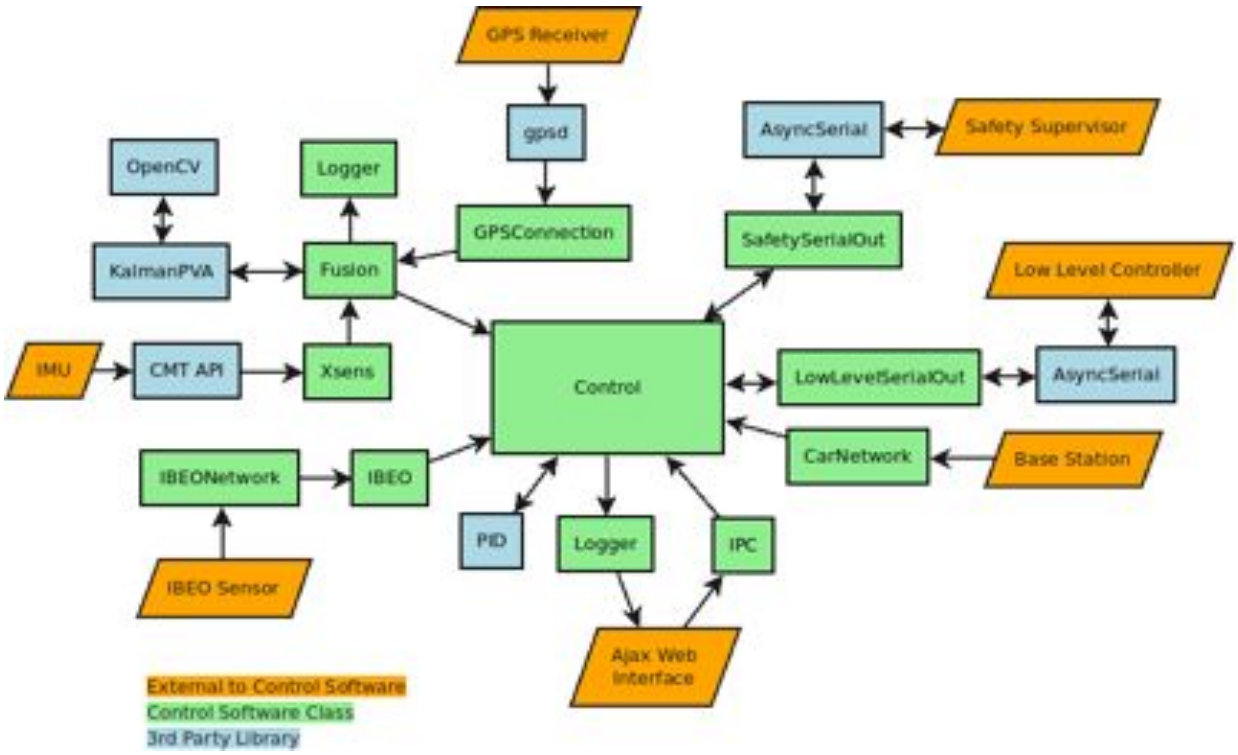

Figure 9: Software topology/data flow diagram

The navigation controller is started by running a shell script which first initialises the *gpsd* daemon, creates a ram-disk, sets the permissions on the various interfaces and then starts the *Control* executable with a negative “niceness” (high process priority). The *Control* executable begins by preparing directories for logging, configuring the terminal display and creating an instance of the *Control* class, before executing the *Control::Setup()* function and then the *Control::Run()* function in which the main thread loops. The *Control* constructor creates instances of all the other required classes which it handles directly and *Setup()* calls the *Open()* function in each which initialises the various interfaces. At the start of *Run()*, the various *Start()* functions are called, creating child threads (by use of the *Boost.Thread* library) which perform each of the classes' IO operations. The program then runs in this state until a *SIGINT* signal is received, at which point each classes clean-up methods are called and the main program exits. A brief description of the functionality of each class module is shown in Table 2 overleaf.

IO Classes	
Name	***Description***
CarNetwork	The CarNetwork class utilises the Berekely sockets API to provide a server for communication with the base station. Messages received are parsed and appropriate functions called to deal with their results.
GPSConnection	GPSConnection uses *libgpsmm* which is part of the *gpsd* suite to communicate with the *gpsd* daemon which receives messages from the GPS receiver. The received data is parsed and calls are made to Fusion member functions to act upon the new position/velocity/heading information.
IBEO	The IBEO class contains Tim Black's [2] implementation of the IBEO Ethernet protocol which decodes the byte stream received via *IBEONetwork* as well as code developed for the Autonomous SAE car which handles processing and acting upon the received data. The received object data is used to project detected obstacles (“fenceposts”) back onto the map current loaded in memory and the scan data is used to for detection of the road edges (see section 4.3). Two sets of files are written out for every 200ms containing the received scan/object data for review and the most recent data is written to the ram-disk for display in the web interface.
IBEONetwork	IBEONetwork was implemented in this project and uses the Berkeley sockets API to connect to the IBEO scanner.
IPC	The IPC (inter-process communication) class creates and listens to a named pipe for commands sent from an interface to the Control program. When each new line terminated command (and comma separated arguments) is received, it is parsed and appropriate action taken.
LowLevelSerialOut	This class uses the *AsyncSerial* library (a wrapper for the Boost.asio library) to communicate with the drive-by-wire controller over a serial port. A constant stream of commands (see Appendix B) are transmitted based on the current set points and received data including command acknowledgement, error codes and informational messages are parsed and acted upon as appropriate.
SafetySerialOut	This class is similar to the above except that it interacts with the hardware safety supervisor module (see section 6.3).
Xsens	The Xsens class uses the vendor-provided CMT API to receive data from the IMU. The data is then processed to provide acceleration and heading data in the correct format for use in the Fusion class.
Utility Classes	
Name	***Description***
Control	The Control class's main loop handles output of information to the terminal display and to a log file located on the ram-disk for use by the web interface. This class also contains the functions used to generate the trajectory for autonomous driving, functions that deal with mapping functionality as well as (static) utility functions which are used in various parts of the program.
Fusion	The Fusion class contains a set of functions which are called when new GPS data arrives and are used to fuse GPS and IMU data in order to produce improved heading and position estimates. This class performs extensive logging of the data it produces and performs a set of actions each time a new estimate is generated.
Logger	The Logger class is used extensively throughout the program for file IO operations. It allows recording of time-stamped data as well as the writing of lock files to indicate when a log is currently being written out.

Table 2: Description of Control program modules.

Base Station Hardware IO Software

The base station software provides three primary features – interfacing with the USB emergency stop button, generating the heartbeat signal and relaying these signals to the navigation controller via a TCP/IP connection over Wifi. The software generates a binary valued heartbeat signal, outputs it to a DATAQ DI-148 USB IO interface and reads two input lines – one which is used to detect the position of the emergency stop button via its NO contacts and another which receives the heartbeat signal via the stop button's NC contacts. The state of the heartbeat read by the DI-148 is then used for transmission to the car. This arrangement allows for instant detection of the buttons position as well as providing a fail-safe verification that the interface is working via the heartbeat signal. In the case that the stop button is pressed, the base station will send an emergency stop command as well as the heartbeat being interrupted (see Appendix C for the wiring diagram).

The ability to control the car using a USB hand controller was also implemented as a secondary feature which was utilised during integration testing of the drive-by-wire system. Two axes of controller are read as well as two buttons (alarm and emergency stop) and sent to the navigation controller via the network link which are then sent to the drive-by-wire controller if the navigation controller is in manual mode. Additionally, buttons are provided in the UI for sending commands to the navigation controller for changing safety profile (see section 6.1), enabling manual mode and emergency stopping the car.

The base station software was implemented in Microsoft C#.NET as a COM/ActiveX control which provides an API for communication with the DATAQ DI-148 was readily available. In addition, the availability of SharpDX, a DirectX API made interfacing with the USB controller via DirectInput relatively simple. The base station UI is a Windows Forms Application and as such is event driven, with events generated by interaction with the form itself, by timers or by the DATAQ ActiveX control. The TCP/IP connection with the navigation controller is established using the .NET *Socket* library and works synchronously, blocking execution until the acknowledgement of each command is received after sending (or a time-out occurs). The command set implemented in the base station software and the navigation controller's *CarNetwork* class are shown below in Table 3.

Command	*Description*
ESTOP	Emergency stop
HBT +	Heartbeat high value
HBT -	Heartbeat low value
BIL	Toggle safety profile
MAN	Set navigation controller to manual control
ALM	Sound piezo alarm
ACL <X>	Set accelerator/brake value to <X>
STR <X>	Set steering value to <X>

Table 3: Base station command set.

Web Interface

The web interface displays data from the main Control program, provides tools for mapping and can send commands and parameters to the Control program. The use of a web-based interface allows for ease of use and a high degree of flexibility but with relatively simple implementation (see section 5.3). Data from the control program is written periodically into a series of files stored on a ram-disk – a file location mounted in RAM which provides fast temporary storage. Files include a listing of various parameters in the Control program, the most recent log information, the map data which is currently loaded and the most recent LIDAR datasets.

The light-weight web-server software *lighttpd* is used to deliver information to the users web-browser via the HTTP protocol. The web pages are written in HTML and are largely static pages, that is, the content does not change after being served. However, a technique known as AJAX has been employed which utilises the JQuery framework to allow for data transfer between the web-server and the browser after the page has loaded, eliminating the need for constant refreshing and the need to transfer all the data at once regardless of need. Scripts written in Perl are used to translate information between the files written out by the Control program into JavaScript Object Notation (JSON) data which can be served by lighttpd to the webpage via the Common Gateway Interface. Similarly, data from the web page is relayed back to the Control programme via a Perl script which writes the data to a named pipe (a POSIX file structure used as a FIFO buffer) which is read in by the IPC module.

4 Sensor Selection and Integration

4.1 Overview

An autonomous vehicle requires an array of sensors which are able to supply data regarding its current position and kinematics as well as knowledge of the environment surrounding it. Reliability, accuracy and sensor coverage are highly important as the information used for navigation is critical to the safe operation of the vehicle and typically an array of sensors is implemented with redundancy and extended capabilities obtained through multi-sensor data fusion techniques. Table 4 below presents a survey of recent autonomous vehicles and their chosen sensors.

	Kinematics			***Environment***		
Vehicle	***GPS***	***INS***	***Odometry***	***LIDAR***	***RADAR***	***Vision***
Clavileño [20]	RTK	Y				Stereo
Junior [9]	D-GPS	Y		5x	5x	
Little Ben [10]	Y	Y		9x		Stereo
MuCAR-3 [29]	D-GPS	Y	Y	Y		Stereo + 1
Odin [11]	Y	Y	Y	7x		
Shelley [22]	RTK & D-GPS	Y				
SLSV [8]	D-GPS	Y	Y	3x		
Stanley [7]	D-GPS	Y	Y	5x	2x	Y
VisLab Van [12]	Y	Y		4x		7x

Table 4: Survey of sensor technologies in autonomous cars.

It was found that advanced GPS systems in combination with Inertial Navigation Systems were most commonly used for measurement of the vehicles heading, speed and position and that LIDARs were the most commonly used sensor for environmental sensing. In this project, in addition to the use of a GPS and Inertial Measurement Unit, a LIDAR was chosen exclusively for environmental sensing due to the high performance available and relative ease with which information can be extracted from the measured data. A web-cam has been mounted above the laser scanner and currently provides a live view of the cars path whilst driving. In this project the camera has only been used for information during testing, however there is significant potential for the integration of image processing into this project.

4.2 Position and Orientation

Global Positioning System

Standard GPS receivers compute their position by measurement of the time differences in receiving "pseudo-range" signals from at least four GPS satellites [30]. Through knowledge of the satellite's orbital parameters this information is used to calculate a position on the Earth's surface. Typically, velocity information calculated by means of the Doppler Effect is also available. When a changing position is detected the GPS module will also report a calculated "track angle", that is, a bearing in the direction of motion.

The accuracy of standard GPS devices has improved over recent years with the cessation of "Selective Ability", upgrades to the satellite constellation and the introduction of more advanced measurement and augmentation systems [30]. Differential GPS utilises ground based stations to broadcast GPS error corrections for localised areas and Satellite Based Augmentation Systems such as the US Wide Area Augmentation System perform a similar function using additional geostationary satellites. Real-Time Kinematic systems utilise a local ground station and determine the relative position between the moving object and the ground station via measurement of the GPS carrier phase – such systems are able to achieve centimetre level accuracy [31].

A variety of commercial products are available which provide built-in sensor fusion as well as functionality including D-GPS correction and RTK measurements. The cost is proportional to the accuracy and ranges from around $1000 for sub-meter accuracy (e.g. D-GPS), to around $5000 for decimetre accuracy (dual channel commercial SBAS) to tens of thousands for advanced survey-grade RTK systems [31]. Products such as the Applanix POS LV which include these high-level features have commonly been used in autonomous vehicles [22][32], however, with no public SBAS available in Australia and systems such as D-GPS and RTK still extremely expensive, a standard GPS device was selected for this project.

The module used in this project is a QStarz BT-Q818X – it possesses a USB interface and sends NMEA 0183 GPS data via a virtual serial port. The GPS unit includes a Li-Ion battery, which allows it to operate continuously independent of the car's power system. The unit is configurable via a PC application and in this project has been configured to send GPSRMC messages at a rate of 5Hz.

Specification	*Value*
GPS Chipset	MTK II
Frequency	L1 1575.42MHz
Channels	66
Antenna	Internal patch (with LNA)
Position Accuracy (no SBAS)	3m
Velocity Accuracy	0.1m/s
Update Rate	1Hz or 5Hz

Table 5: QStarz GPS-818X Specifications. Source: [33]

Experiments were conducted to gain further knowledge about the position information reported by the GPS module. Two identical receivers were placed approximately 30cm apart and left for 40 minutes, recording data at 5 Hz whilst stationary. The results shown in Figure 10 have been converted to metres relative to the centre-of-mass. A mean deviation of 1.45m with a standard deviation of 0.94m and maximum of 4.5m was recorded. As the RAC DTEC race course is around 7.5m wide, this sensor is clearly not sufficient to always keep the car constrained to the roadway and so these results display a need for a more accurate and reliable system for positioning.

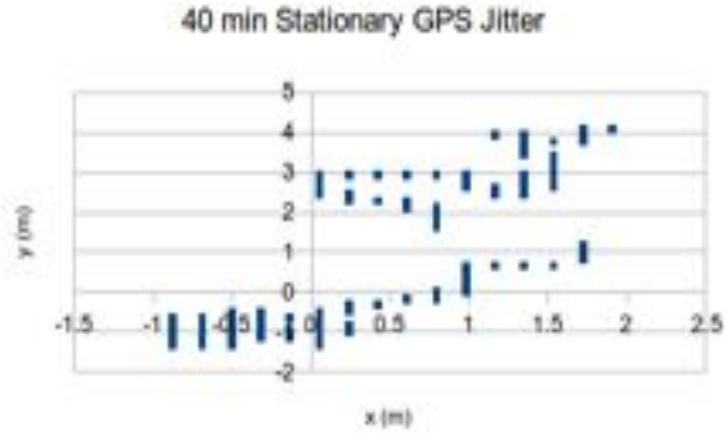

Figure 10: Results of GPS Static Jitter Measurement

It was hypothesised that differential error correction could be used by having one GPS receiver stationary and using it to subtract error from an identical unit on the SAE car. Unfortunately, the results of these experiments showed that such a scheme is not possible, as the jitter is not able to be reliably correlated (see Figure 11). This is most likely due to the inability to guarantee which satellites have been chosen to form the position estimate by the filtering algorithm internal to each GPS. Approaches have been presented for local differential GPS [34], however a receiver which can output the raw pseudo-range data from the satellites is required so that all processing can be done external to the GPS units internal filter. The GPS receivers used in this project do not support this and significant effort would need to be invested in making such a scheme operate reliably over a wireless link.

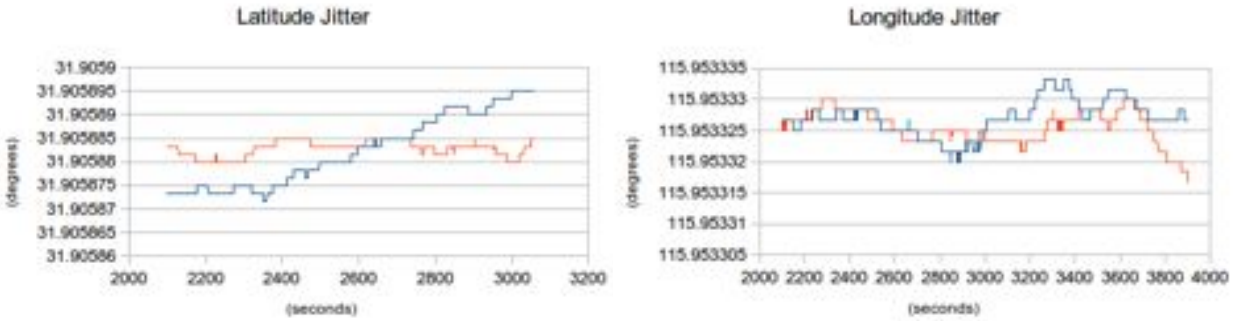

Figure 11: Comparison of jitter of two GPS modules.

Inertial Measurement Unit

An Xsens MTi IMU is used in this project in order to improve the accuracy and frequency of the data provided by the GPS. The unit combines a magnetometer, MEMS 3D accelerometer and MEMS gyroscopes and is designed to output Kalman filtered orientation data for use in the stabilisation and control of robots and vehicles [35]. Calibrated (against the manufacturing imperfections of the sensor) inertial data consisting of acceleration, angular velocity and magnetic field readings are also available from the sensor. In this application the filtered orientation data and calibrated accelerometer data are used.

Type of Data	***Specification***	***Value***
	Update Rate	Up to 256 Hz
Orientation	Angular Resolution	0.05°
	Repeatability	0.2°
	Static Accuracy (roll/pitch)	0.5°
	Static Accuracy (heading)	1.0°
	Dynamic Accuracy	2° RMS
Acceleration	Linearity	0.2%
	Bias stability	0.02 m/s^2
	Scale factor stability	0.03 m/s^2
	Noise Density	0.002 $m/s^2/\sqrt{Hz}$
	Alignment Error	0.1°
	Bandwidth	30 Hz
	Resolution	2^{16}

Table 6 Xsens MTi Specifications. Source: [35]

Early investigations showed that the accelerometer data is too noisy to integrate directly with the calculated position diverging in just seconds. The filtered heading data is reasonably good but tests have shown that it is prone to errors introduced by magnetic field disturbances, particularly when used on the SAE car. To this end an aluminium bracket was constructed in order to keep the sensor clear of the steel tube and electrical systems present almost everywhere in the car (see Figure 21 in section 3.4). Unfortunately this placement of the sensor is non-ideal with respect to

collecting inertial data (ideally the sensor would be placed in a stable position near the centre of mass), however, the configuration has proven delivered far better heading measurements. Software provided with the sensor was used to calibrate the sensor after installation on the car by driving in circles in order to map the local magnetic field. Before construction of the aluminium bracket, it was not possible to achieve a result from this process but an expected accuracy of 0.9 degrees was achieved with the bracket installed (see Figure 12).

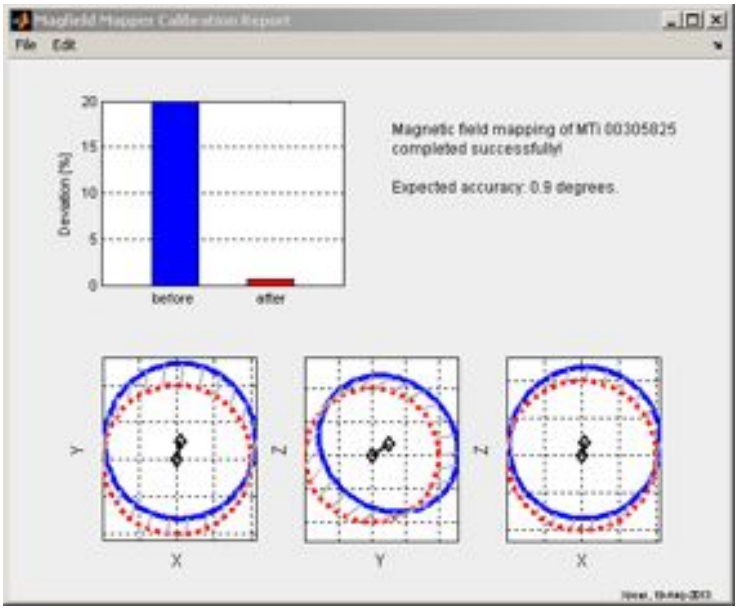

Figure 12: 3D Calibration of IMU using manufacturer's software.

Sensor Fusion

Sensor fusion refers to techniques used in multi-sensor control systems in order to improve the reliability, quantity and accuracy of measured information [36]. In particular, sensor fusion algorithms often possess fault tolerance [37] or utilise statistical or Bayesian techniques in order to improve the confidence in measured values [38]. The applications of sensor fusion are vast and can be as simple as the use of additional instruments to provide verification of measurements in a laboratory setting or more complex with applications in wide-area sensor networks, robotics and navigation [36].

Fusion of GPS receivers with an INS or IMU is a common amongst systems designed for use in moving vehicles. GPS data is filtered and combined with inertial measurements to ensure that the position estimate is accurate particularly during periods of poor GPS signal availability [32], though such techniques do not guarantee absolute position accuracy. High-end commercial GPS units often incorporate the IMU and fusion algorithms in one device (e.g. [32]), however, a mid-level device, the Xsens MTi-G-700 was identified as an ideal replacement for the Xsens

MTi and QStarz GPS receiver used in this project. The MTi-G combines an Xsens IMU with a good quality GPS receiver featuring an external antenna and incorporates a proprietary sensor fusion algorithm which can create position, velocity and orientation estimates at up to 400 Hz [39]. Unfortunately, it was not possible to obtain the device for inclusion in the project and so sensor fusion techniques were investigated at the navigation controller level.

Vehicle Heading

Fusion of the IMU heading and GPS track angle measurements was found to be required due to the speed dependent accuracy of the GPS track angle (heading) measurement and the limited absolute and dynamic accuracy of the IMU. If the car is not moving at an appreciable rate the reported GPS track angle will not update and substantial jitter was observed at low speeds posing a particular problem in telling which way the car is facing when starting an autonomous drive. In order to determine the extent of this issue data was collected by driving in a straight line (directly south) for approximately five minutes whilst varying the cars speed and starting/stopping on multiple occasions. A total of 1424 samples of speed and GPS heading were obtained and the resultant deviations from the mean heading angle over the drive were then binned according to speed and found to be normally distributed (e.g. Figure 13). The standard deviations with respect to the population mean were then determined for each bin, as well as the standard deviation of the IMU heading over the test and plotted together as shown in Figure 14.

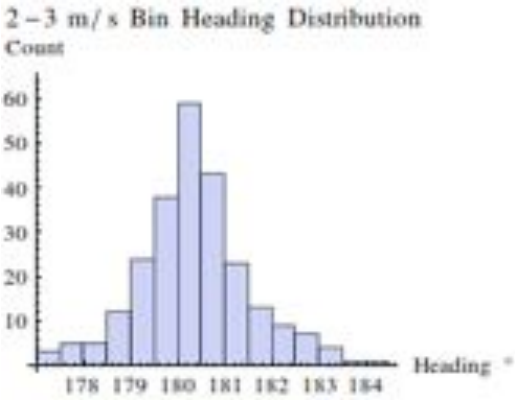

Figure 13: Histogram showing distribution of heading data within a speed bin.

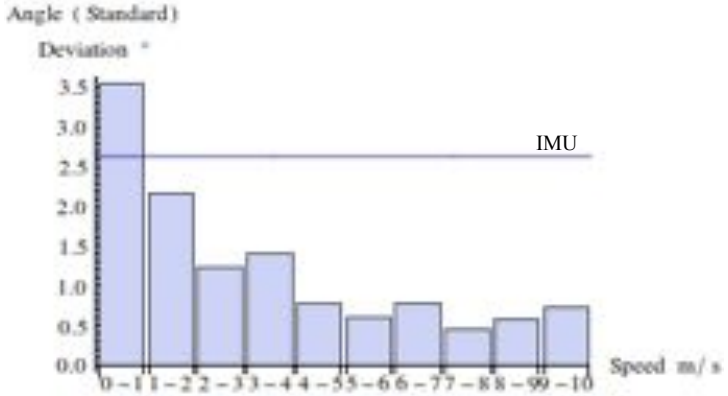

Figure 14: GPS angle standard deviation vs. speed and IMU standard deviation over trip.

The GPS heading data shows a clear speed dependence, with poor accuracy at low speeds and levelling off above 4 m/s. The IMU standard deviation over the same trip was 2.6° with the calibration routine having estimated an accuracy of 2°, however with the IMU mounted on the SAE car's bracket estimated accuracies around 1° are quite achievable. A considerable risk exists in relying on IMU data as magnetic disturbances can cause result in a loss of absolute accuracy

and a “wandering” heading and though the aluminium bracket appears to have prevented this occurring on the SAE car, the phenomenon was observed several times during testing.

A speed-dependent weighted average with characteristics based on these observations was therefore implemented in order to ensure that the most accurate heading at all speeds. Such an approach is based upon the algorithm presented by Elmenreich [38] but with a variable rather than static weighting. The fundamental premise of sensor fusion is to improve the accuracy of a measurement by means of combination of data from multiple sensors and in this case we seek to minimise the variance of the measured vehicle heading. By deriving weightings for the measurements of each sensor, we can create a measurement with lower variance than that of the sensors taken individually. Treating the GPS and IMU as random variables X_G and X_I respectively we can model the fused measurement as a Gaussian random variable where $Z = w_G X_G + w_I X_I$.

Then, applying the method of Elmenreich [38] to this specific case we can first use the fact the variables are independently Gaussian distributed to give the combined variance:

$$\sigma_Z^2 = w_G^2 \sigma_G^2 + w_I^2 \sigma_I^2$$

Since Z is a weighted average and we require $E[Z] = E[X]$:

$$w_G + w_I = 1$$

We then seek to extremise σ_Z^2 by setting both partial derivatives to zero:

$$\frac{\partial \sigma_Z^2}{\partial w_G} = \frac{\partial}{\partial w_G}\left[w_G^2 \sigma_G^2 + (1 - w_G)^2 \sigma_I^2 \right] = 2 w_G \sigma_G^2 - 2(1 - w_G)\sigma_I^2 = 0$$

$$\frac{\partial \sigma_Z^2}{\partial w_I} = 2 w_I \sigma_I^2 - 2(1 - w_I)\sigma_G^2 = 0$$

Checking the second derivatives it is clear that:

$$\frac{\partial^2 \sigma_Z^2}{\partial w_I^2} = 2\sigma_I^2 + 2\sigma_G^2 > 0 \ \wedge \ \frac{\partial^2 \sigma_Z^2}{\partial w_G^2} > 0$$

Giving:

$$w_G = \frac{1}{1 + \frac{\sigma_G^2}{\sigma_I^2}} \ , \ w_I = \frac{1}{1 + \frac{\sigma_I^2}{\sigma_G^2}} \ \Rightarrow \ \sigma_Z^2 = \frac{1}{\frac{1}{\sigma_G^2} + \frac{1}{\sigma_I^2}}$$

These formulas were then used to calculate the value of the weighting factors in each of the speed bins (shown by the points in Figure 15). The calculated standard deviation for the combined system is shown overlaid in Figure 16 and has had most effect (32% decrease) in the 0-1m/s bin, with smaller, but noticeable improvements up to around 4m/s. For implementation on the car system a piecewise linear function (see Figure 15) was used as an estimation of the weighting factors, although modifications were made to ensure that the GPS heading was not included in the average at speeds less than 0.5 m/s. As there is the potential for GPS errors up to 180° when commencing driving from stationary it is not appropriate for it to be used at all in the weighting at very low speeds.

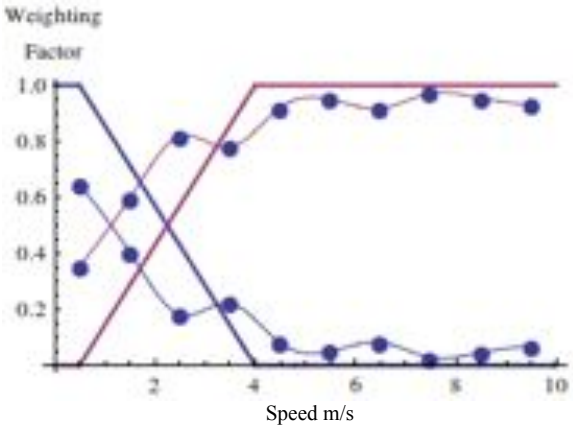

Figure 15: Heading measurement weighting values (blue – IMU, maroon - GPS).

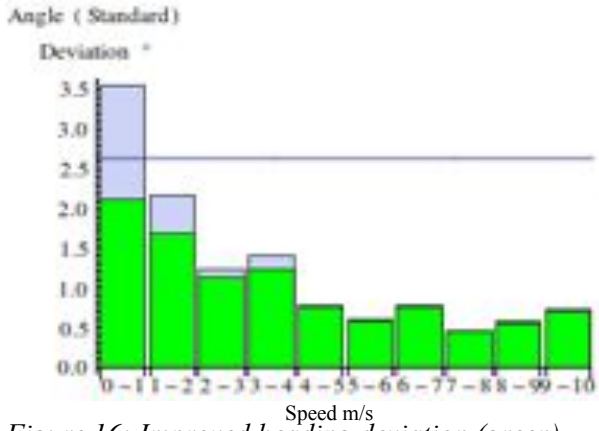

Figure 16: Improved heading deviation (green).

It is important to note however that in the case of non-straight line operation the GPS reports the car's “track angle” (i.e. the direction it is currently moving) whilst the IMU outputs the direction the car is current facing. In order to determine the cars trajectory the track angle is required and a correction is made to the IMU heading value based on the angle at which the front wheels are being steered. This was determined by establishing the relationship (see Figure 17) between the byte values sent to the drive-by-wire controller and the actual wheel angle. A further limitation is that the car is not guaranteed to travel in the direction of the wheels when a lateral force is present a “side-slip” condition occurs, leading to a deviation between the wheel angle and track angle (as shown in Figure 18). However, in this project the IMU heading and its associated correction are only utilised at very low speeds and so it is unlikely that this effect will cause any significant issues.

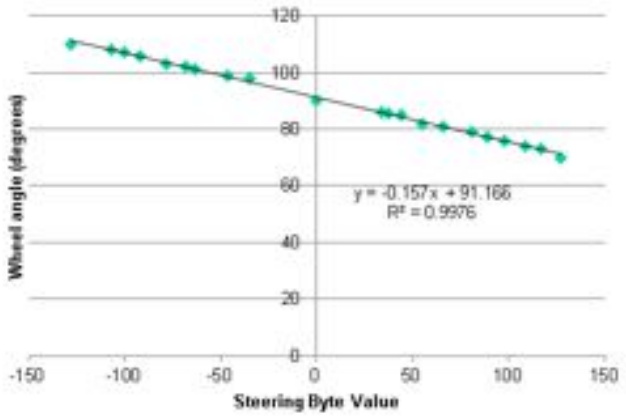

Figure 17: Characterisation of drive-by-wire steering controller.

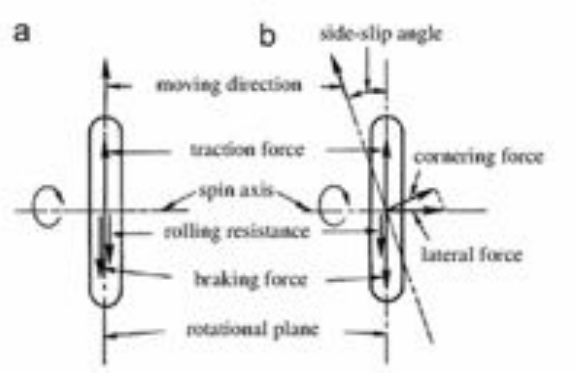

Figure 18: Non-slipping (a) and slipping (b) tyre models. Source: [40]

There is also a desire for more frequent heading updates and so the high-rate IMU data is used to interpolate the calculated heading. By measuring the short-term heading change using the IMU between receiving GPS data and an intermediate time before the next set of GPS data an intermediate heading value is obtained. By using only the change in heading reported by the IMU, bias type error associated with the IMU heading does not affect the interpolated points or cause inconsistency with the fused heading data. At present this method is used to increase the heading update rate to 10 Hz, though higher rates are possible if desired.

Positioning

A filtering algorithm based on the Kalman Filter has been implemented in order to smooth and improve the accuracy of the car's positioning data. The Kalman Filter was first presented in 1960 and is used to create refined estimates of a system state based upon knowledge of the state transition and control matrices which describe the system (A, B respectively) and the covariances associated with the noise processes inherent to the system and sensors [41]. Measurements may be taken of the system using one or more sensors as described by H, the measurement matrix, with covariance matrix R, whilst Q describes the covariance(s) of the physical process itself. In the case of a discrete-time Kalman Filter, at each time step the current state of the system and the associated error covariance is predicted using the system model. The Kalman gain K matrix is then calculated and used to combine the measured and estimated states in such a way that the new error covariance is minimised. This process can be expressed diagrammatically, as shown in Figure 19.

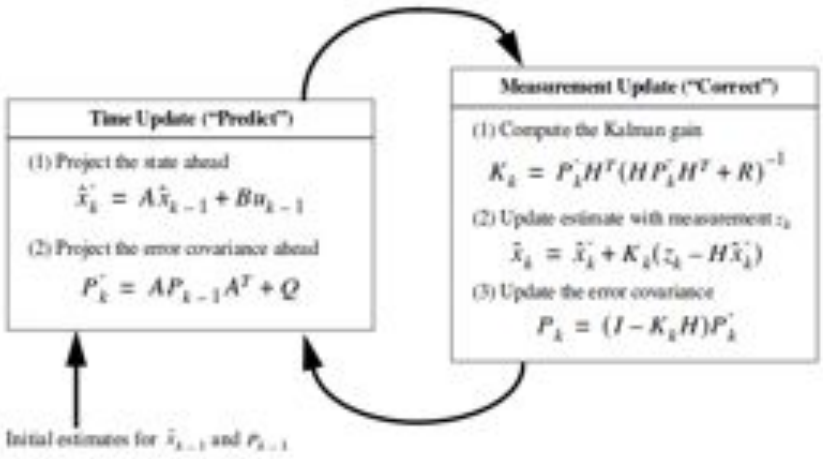

Figure 19: Kalman filtering sequence. Source: [41]

The concept of applying such a filter to a GPS/INS system is based upon the observation that GPS error, though bounded, is large and may have reliability issues whilst INSs possess a small error over small time-scales and are not subject to the same error sources as GPS [42][43]. Significant work has been conducted into the field of GPS-INS fusion and the standard methodology utilises the Extended Kalman Filter or another other non-linear filtering method in a "tightly coupled" configuration in which INS measurements are integrated with the GPS receivers filtering algorithm [44]. Loosely couple algorithms have also been investigated and utilise the outputs from the INS and GPS devices internal filters but provide feedback to the INS integration filter allowing the INS integration error to be "reset" or offset by the Kalman filter's output [43]. The class of algorithm investigated in this project is a direct loosely coupled approach in which the acceleration output from an IMU and position and velocity outputs from the GPS are combined directly.

Benefits of direct loosely coupled algorithms include relative simplicity, the ability to use linear filtering techniques, low computational load [45] and the ability to use inexpensive sensors such as those available in this project [42] whilst maintaining competitive performance. In the algorithm implemented for the Autonomous SAE Car, the acceleration data is first transformed into a North-East-Down coordinate system using orientation data read as a cosine matrix from the IMU. It is then averaged over the last fifth of a second and combined in a second order Kalman Filter with the GPS (Doppler) velocity information. The estimated velocity from this filter is then combined in another second order Kalman Filter with the position data, which is then used to compute the cars trajectory. Both filters currently use a linear free body model for the system, though there is scope for a more advanced model to be investigated in the future. An

estimation of the velocity and position in between each set of GPS data is created by prediction based upon the free body model and the most recent acceleration data, increasing the update rate of the position and velocity information to 10 Hz.

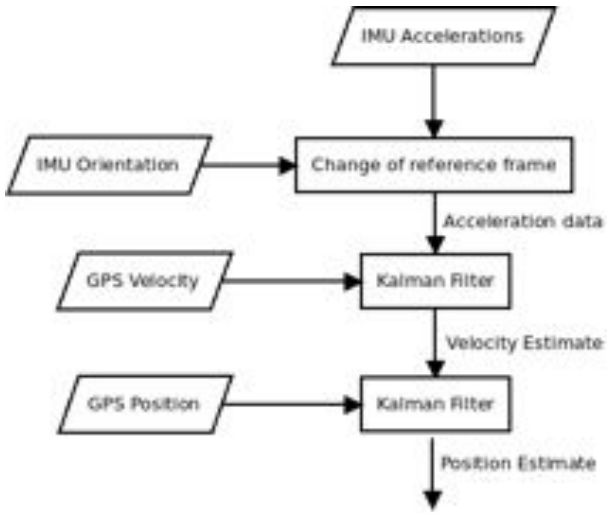

Figure 20: Position/velocity fusion algorithm

4.3 Physical Environment

IBEO LIDAR

The LIDAR system used in this project consists of an IBEO Lux automotive LIDAR. This sensor utilises reflected infra-red light in order to measure distance (via time-of-flight) and can build a 3D point cloud by scanning horizontally in four vertical layers. The IBEO sensor has sophisticated internal data processing functionality including object detection and classification. Data is delivered using TCP/IP over an Ethernet connection and includes scan data in polar coordinates and object data in x-y coordinates referenced to the sensor.

Specification	***Value***
Technology	Time of flight (output of distance and echo pulse width)
Range	200m
Field of View (Horizontal)	85°
Field of View (Vertical)	3.2°
Layers	4
Echo Detection	3 measurements per pulse
Update Rate	12.5/25/50Hz
Accuracy	10cm

Table 7: IBEO Lux LIDAR Specifications, Source: [46]

In this project the sensor was mounted on a specially constructed bracket above the car's roll cage. Vertical angle adjustment is provided so that the sensor can be positioned and locked in the optimal orientation. In particular, when used to determine the position of the road it is necessary to angle the sensor down slightly. The mounting was constructed from tubular steel and is secured to the chassis in three points – the base of the frame slides into supports welded to the car's frame and a cross-bar attaches to the top of the roll hoop in order to provide a stiff mounting and minimise vibration. The sensor itself is mounted on a piece of waterproof fibreboard and attaches to the frame via saddle clamps attached to the top cross-bar. Acrylic locking segments located at the bottom edges prevent the sensor angle from changing due to vibrations whilst driving.

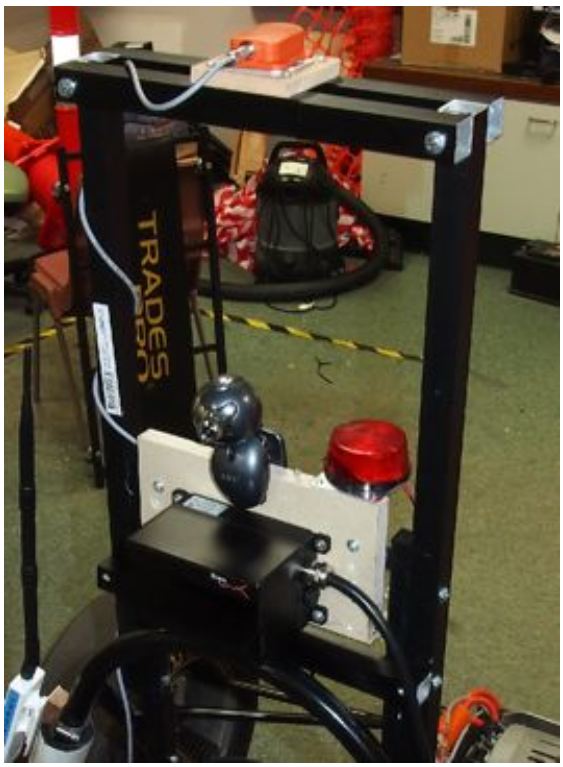

Figure 21: IBEO/IMU mounting bracket

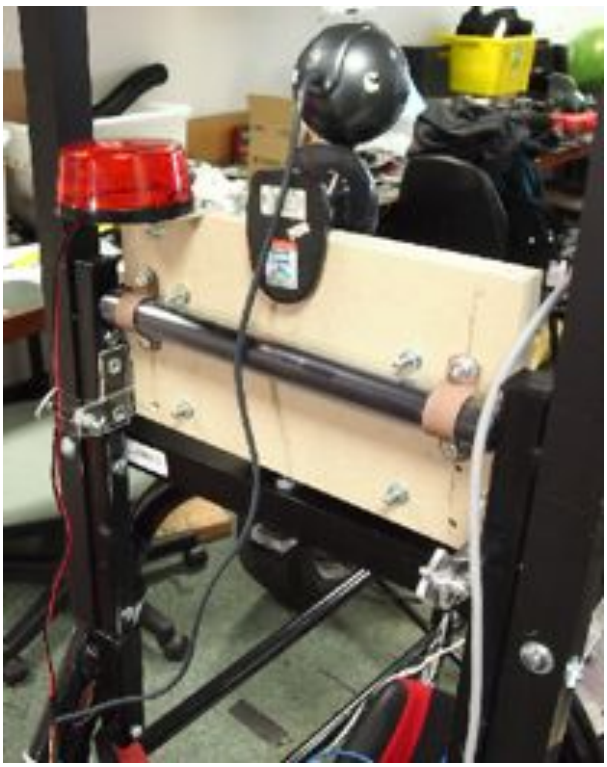

Figure 22: Adjustment locking mechanism

Road Edge Detection

Prior research has been conducted on road edge detection both through optical systems [19] as well as through the use of LIDAR sensors such as in the winning entry in the 2007 DARPA Urban Challenge [24] and in research at German [25] and Singaporean [26] universities. The methodology described in [24] utilises a feature-extraction algorithm based upon location of local maxima and minima in the LIDAR data as well as the variance of segments between these extrema. Other algorithms such as [26] rely on the presence of curbs and seek to identify and track curbs as features in the LIDAR data. The approach described in [25] is similar to the initial

algorithm employed here and attempts to seek appropriate linear fits to the road surface, however their estimates were then combined with filtered reflectivity data in order to find the road surface. In both of the latter two cases a Kalman filter is used to track the position of the road edges temporally.

In this project the IBEO sensor's "scan data" sets consisting of polar angle/radial distance pairs were analysed in order to find the horizontal extent of the road surface. By mounting the sensor at height (i.e. above the roll cage) the sensor plane intersects the road in such a way that radial distance variations are recorded for both variations in the height of the road/curb as well as in the distance in front of the car (see Figure 23). It was found during experimentation with the IBEO sensor that observed that road points on a bitumen surface tend to be arranged collinearly with a small deviation whereas points belonging to uneven surfaces (such as grass and curbs) tend to be scattered, with their arrangement depending on the contour of the surface away from the road edge.

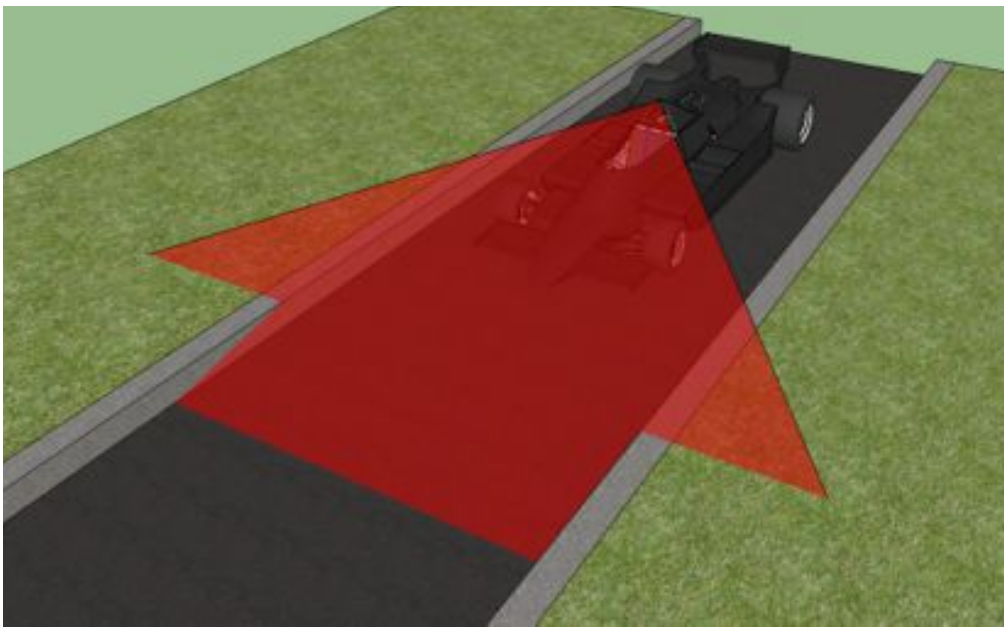

Figure 23: LIDAR edge detection geometry.

In the case of the Autonomous SAE car, detection which relies upon the presence of curbs or marked lines is not feasible as race tracks, unlike public roads may not have such features (in particular, the RAC DTEC track has grass/dirt edges). In addition, the algorithm must be able to dynamically detect road edges whilst the car is moving (and turning) and should have an accuracy better than 0.5m at each side. The algorithm developed here therefore focuses on identifying the presence of a road section rather than the presence of a particular edge characteristic and will thus work both on curbed and non-curbed roads.

The following hypothesis was developed for the detection of road edges:

Roads should be:	Mostly, but not always close to the centre of the scan
	Smooth (e.g. points co-linear)
	In the same plane as the car (e.g. small horizontal gradient)
Edges may be:	Scattered (non-linear)
	Sloped
	Raised/lowered

An additional property, considered later, is that the road-edge boundary should be locatable in a predictable fashion over time.

The algorithm implemented in this project operates by first identifying a candidate group of points close to the centre of the scan data which meet the slope condition (i.e. the slope of a line through these points is less than a pre-set value). This group is then expanded iteratively, with a least-squares linear regression performed at each step. By minimising the square residuals between the fit line (*y)* and the data (x_i,y_i), this technique obtains the most appropriate line for the given data set, the success of which can be measured by means of the product-moment correlation coefficient *r*. In this case, the slope (*b*) and r^2 values are of relevance and are tabulated.

$$\text{Specifically;} \quad y=(\bar{y}-b\bar{x})+bx \quad , \quad r=\frac{s_{xy}}{s_x s_y} \quad \text{where}$$

$$b=\frac{s_{xy}}{s_x^2} \quad , \quad s_{xy}=\frac{\sum_{i=1}^{n} x_i y_i}{n}-\bar{x}\,\bar{y} \quad , \quad s_x^2=\frac{\sum_{i=1}^{n} x_i^2}{n}-\bar{x}^2 \quad , \quad s_x^2=\frac{\sum_{i=1}^{n} y_i^2}{n}-\bar{y}^2$$

This technique is performed independently for the left and right hand sides of the candidate point group to allow for the fact that roads are often sloped about the centre (e.g. to let water run off) which results in improved accuracy. In the initial implementation, the road-edges were then determined to be the outer edges of the candidate groups which maximised the respective correlation coefficients and met the slope condition. In summary, the algorithm follows this sequence:

1. Step out from the centre of the dataset looking for a point cluster which meets the slope condition. Interleave looking to the left and right.
2. Perform stepping to the left and right (seperately) of this cluster , increasing the size. Fit lines and record the slope and correlation coefficient (r^2) at each step.

3. Road edges are at the point which maximises r^2 whilst meeting the slope condition.
4. Calculate overall fit line and check that the slope and correlation conditions are met.

Two examples showing captured scan data with the identified road segment lines and a photograph of the respective scenarios are shown below in Figure 24. In the first example the car is positioned with a wall to the left and a grassed area to the right. The sensor has been angled downwards to give a small field of view with the LIDAR scan plane hitting the ground around 4m from the car. The algorithm has correctly identified the road surface based on the linearity alone, highlighting the variety of edge scenarios supported by this algorithm.

The second example is substantially more challenging and shows a brick path with an undulating section of grass to the right and a garden with trees to the left. The sensor has been positioned to measure the ground some 20m out and so the path occupies a very small section of the horizontal span and the uneven bricks result in scatter which further increases difficulty. The road area has again been successfully identified despite the increased difficulty in this scenario.

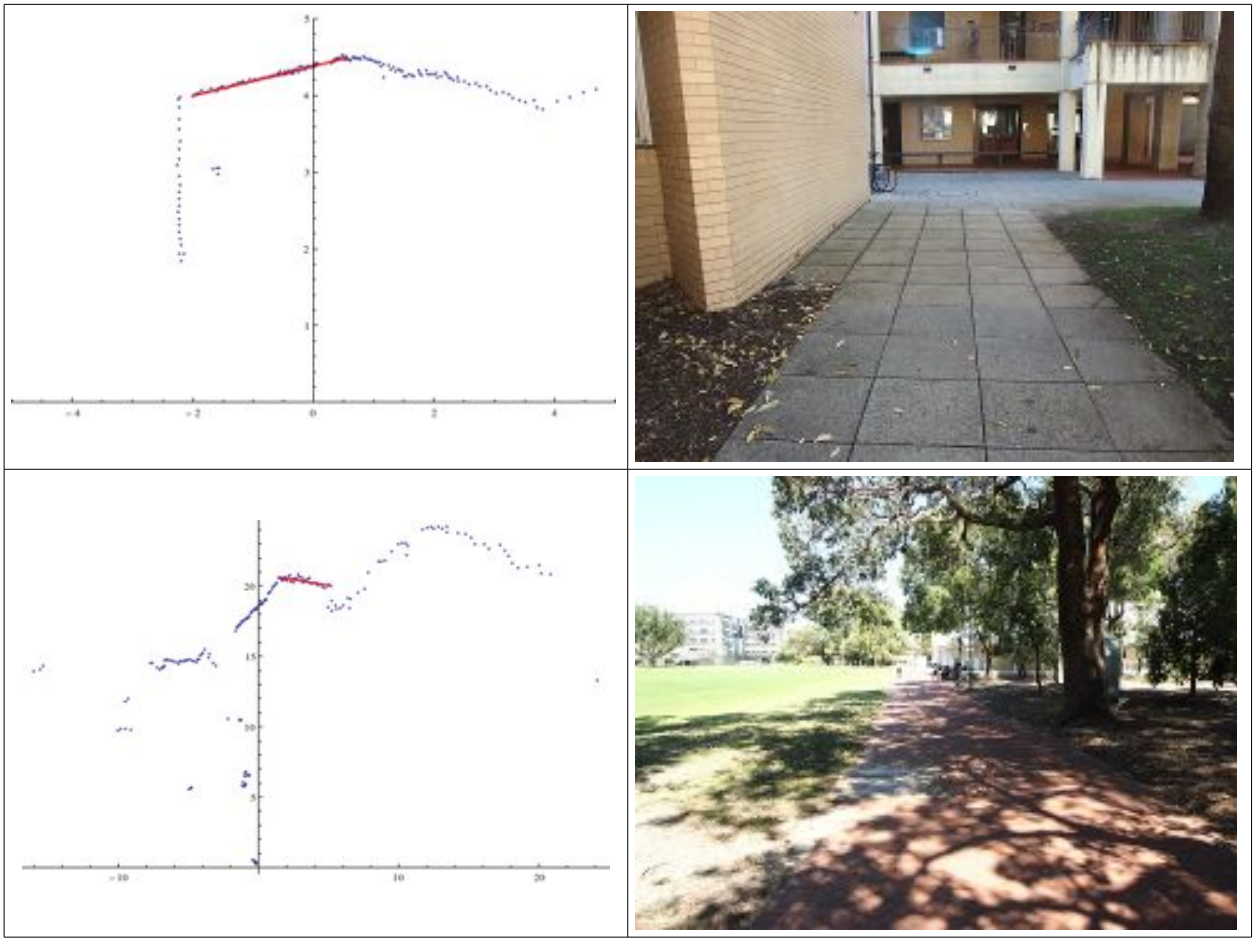

Figure 24: Samples of road-finding algorithm output (LIDAR scan data looking forward from the car's driving position, distance in metres).

It was found, however, that this algorithm did not meet the required performance criteria in terms of correct identification of the edge and consistency whilst in motion. As a result, a more advanced algorithm was developed, which has the same basis as the one described above but with some heuristic intelligence added to the identification of the correct edge value based upon the correlation coefficient data. Central to this approach was the implementation of a Kalman filter [41] which is used to create a time averaged estimate of the road-edge position which can then be used to assist in location of the current road edge. The second order Kalman filter implemented has the following state transition equation and observation matrix:

$$\begin{bmatrix} x_n \\ v_n \end{bmatrix} = \begin{bmatrix} 1 & \Delta t \\ 0 & 1 \end{bmatrix} \begin{bmatrix} x_{n-1} \\ v_{n-1} \end{bmatrix} \quad , \quad H = \begin{bmatrix} 1 & 0 \\ 0 & 0 \end{bmatrix}$$

Thus, a position measurement, x, is provided to the filter and the lateral velocity, v, of the road-edge is a quantity derived within the filter. This approach allows for the estimation of the road edge whilst it's horizontal position relative to the car changes, for example when the road or car deviate from a straight line during cornering or “lane changing”.

The filtered road-edge position estimate is then used in order to improve the accuracy of the identification of the road-edges from the r^2-x data set. The local maxima are identified using the criteria: $max(x) = x_i > x_j \; \forall \; x_j \in [x_{i-k/2}, x_{i+k/2}]$ where k is number of points that a maximum must exceed and is conveniently set to the size of the candidate groups used initially in the algorithm. This information allows a more appropriate maximum point to be selected if desired and also allows selection of the value which makes the road segment largest should the absolute maximum peak be rather broad. It was also observed that much of the time a significant “dip” in correlation was observed at the point when the group was expanded to begin to include features outside the road-edge, giving a second indicator for the position of the road-edge. Thus, four modes for selection of the road-edge were implemented and a pre-set quantity the allowed deviation introduced:

1. If the value that gives the absolute maximum is different by a quantity exceeding the allowed variation, attempt to find the local maximum closest to the current estimate. If it is not possible to find a clear local maximum, attempt mode 2.
2. If the value that gives the absolute maximum is different by a small amount, but less than the allowed deviation and is to the inside of the absolute minimum, return the value of the absolute minimum correlation.

3. If the greatest local maximum peak meets the minimum correlation requirement, return the point at which it is located.
4. If it was not possible to find a reasonable edge candidate, return failure.

Examples of cases in which these modes were applied are shown below in Figure 25. The yellow lines indicate the current estimate used, the green diamonds the identified road-edge point and red points exceed the slope condition.

1 – Reallocated peak	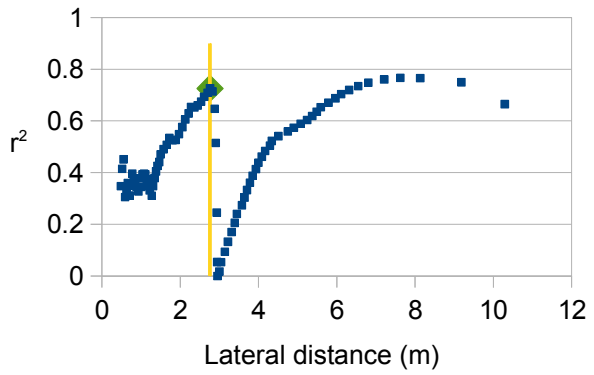
2 – Dip selected	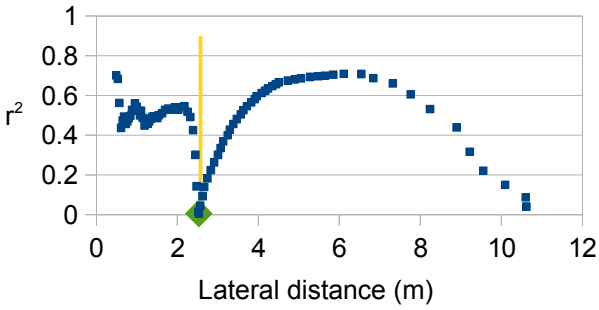
3 – Greatest local maximum peak	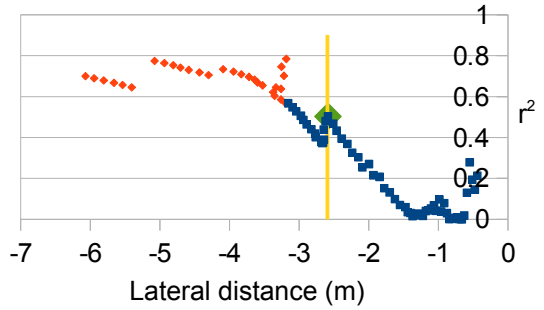

Figure 25: Examples of road-edge identification scenarios.

The most important pre-set parameters for this algorithm are the slope condition value and allowed variation. The slope condition is set based upon the the nature of the road surface and severity of roll experienced – a lower value is preferable and values in the range 0.2-0.3 are typical. The allowed variation is generally set at around 1.5m but may be increased if there is significant expected variation in the road edge position. Limits are placed on the distances both transversely and laterally as to how far away edges should be found and are set based on the sensor orientation. Finally, other parameters including the candidate group size and minimum correlation have been set based upon testing and have been found to be non-critical and do not need any adjustment based upon driving conditions etc. With this improved algorithm it has been observed that fine tuning of parameters is generally not required beyond a first approximation.

Mapping of Obstacles

The IBEO sensor also provides automated object detection and classification and provides information including the objects location, geometry, type, age, velocity and echo point set. This data is projected onto the car's running map data as "fence posts" in order to mark obstructions in the path. Despite the sensor returning the a defined centre point for the object, it is the object echo point data which is used for this purpose, as it reveals more about the shape of objects than the simple rectangles generated by the sensor. As the object data returned by the sensor is Cartesian and relative to the sensor itself, a rotation matrix is used to first change the reference frame before it is project onto the map. Note that the rotation matrix is transposed as the IBEO notation is opposite to the usual convention. The object point is thus located at:

$$\vec{O}' = \begin{bmatrix} \sin(\theta) & -\cos(\theta) \\ \cos(\theta) & -\sin(\theta) \end{bmatrix} \vec{O} + \vec{r} \quad \text{where} \quad \vec{r} \quad \text{is the car's current position vector.}$$

In order to minimise the quantity of data projected, echo points are replaced by "fence post" circles of fixed radius which mesh together. The loss of precision in mapping is not of concern in this application since a safety factor in the order of metres is set with regards to detection of obstructions. The example shown below in Figure 26 shows the detection of building features outside of the laboratory. At the top left the objects are shown with red markers at their centres with bounding rectangles overlaid on the raw four-layer scan data (red, orange, yellow, green respectively) and a detected "road" segment (white) whilst the reduced data set is shown to the top right.

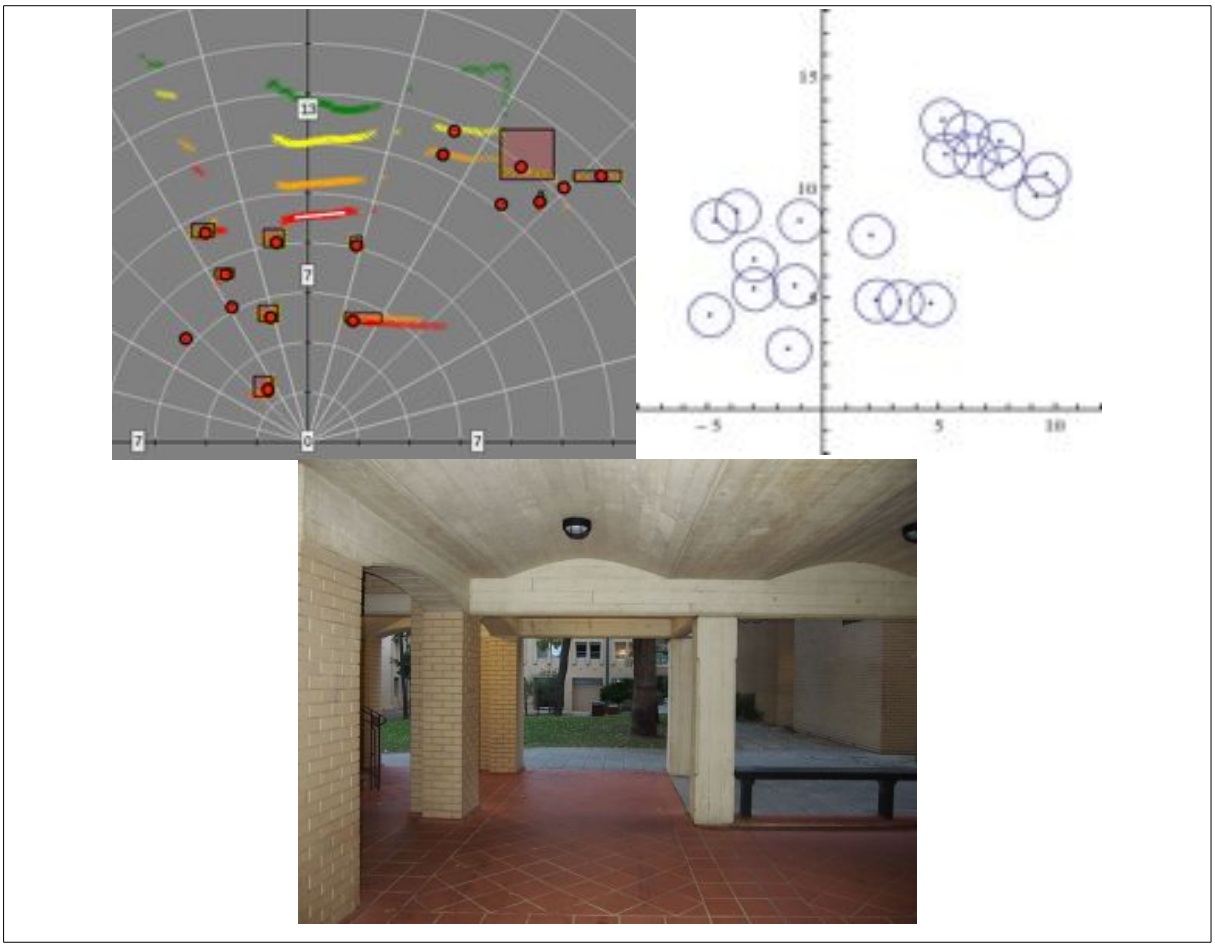

Figure 26: IBEO sensor data (object centres and bounding boxes overlaid on raw scan data), reduced object data, photograph of scenario. All distances are in metres.

5 Instrumentation and Control

5.1 Mapping

Geodesy

In this project, the concept of a "map" is used in order to direct the Autonomous SAE car along a path made up of waypoints. The map format employed here begins with specification of a datum - a latitude/longitude pair which is the origin of a local x-y coordinate system. The maps contents are then specified as x/y pairs in metres relative to the datum, with the y-axis aligned North-South and the x-axis aligned East-West. It is therefore essential that the distances calculated on the Cartesian surface bare some resemblance to reality for both informational purposes and for combination with other data sources. A simplified transformation is used to convert latitude/longitude inputs, φ and λ respectively, (e.g. from GPS or Google Maps) into local Cartesian coordinates:

$$x = R_E \frac{2\pi}{360}(\varphi - \varphi_D)$$
$$y = R_E \frac{2\pi}{360}\cos|\varphi|\,(\lambda - \lambda_D)$$

This approach assumes that the Earth's radius is sufficiently large and the angle difference between the datum and position are sufficiently small that the curvature of the Earth is negligible in the area local to the Cartesian coordinate system. The accuracy is thus proportional to the accuracy of the Earth's radius, R_E, which is defined in the World Geodetic System 1984 [47] (the standard utilised by GPS) to be that of an ellipsoid with equatorial semi-major axis 6378.137 km and flattening factor 298.26. This gives a variation of 21.4 km from minimum to maximum radius, which corresponds to a 0.34% error, which on the scales (100m) used in this project would translate to a maximum error of 34cm. However, a better estimate of the local Earth radius can be obtained based on the geometry of the ellipse:

$$R = \sqrt{\frac{(a^2\cos\varphi)^2 + (b^2\sin\varphi)^2}{(a\cos\varphi)^2 + (b\sin\varphi)^2}}$$

This gives approximately 6372km and was taken as the value of R_E in this project. The error between the WGS84 ellipsoid and the mean-sea-level is on the order of tens of metres [48], as is the local (Perth coastal plain) [49] height above mean-sea-level which is relatively small with respect to the magnitude of the Earth's radius. If a worst case error of 100m was assumed this now corresponds to an error of 0.0016% which quite clearly acceptable in this project.

Implementation

In addition to waypoints, a map can also contain “fence posts” which define an area with an obstacle or boundary that the car is not allowed to come near to. For example, by placing these points around the area in which the car is to be operated as a “fence”, any control failure or inaccuracy that results in contact with these markers will result in the car coming to a prompt stop. Both types of points are operated with a globally defined “radius” which sets the accuracy required before the car is considered to have reached a point which in operation has been set at around 2m, although performance measurement has indicated there is scope for lowering this value.

The maps themselves are portable and stored in files as lists of comma-separated values (CSV) which both the control program and web interface are able to read and write to. Waypoints may either be placed by clicking on a Google Maps display in the web based interface or by automatic recording accomplished by first driving the desired path manually. Recording is initiated via the web interface and records points at constant distance intervals during driving after which the captured map can be written to a file.

Figure 27: Waypoint data recorded automatically and overlaid on the Google Maps interface.

5.2 Trajectory Calculation and Driving

Overview

The autonomous car navigates based upon driving through the mapped waypoints in sequence, with closed loop control systems controlling the heading and speed required in order to complete the path successfully. When autonomous driving is started, the car drives from its current position towards the first waypoint and continues along the path until the final waypoint is reached, at which point the car brakes to a halt and turns off the autonomous control mode. A

waypoint is deemed to have been reached when the cars current position is within a certain distance of the waypoint, the waypoint radius. Ideally, the size of a waypoint would be quite small, however, the use of a larger point increases the likelihood that the car is able to successfully reach the point.

Two primary classes of trajectory generation are found in mobile robotics [12]; Sliding Mode Path Following involves the pre-generation of the path to be driven and the use of controllers in order to keep minimise the lateral deviation from the vehicle's current position to the path centre (e.g. [7]) whilst dynamic path following methods (such as Traversability-Anchored Dynamic Path Following) continuously recalculate the trajectory based upon the vehicle's current location and consideration of the environment ahead (e.g. [29]). The algorithms presented here are of the latter variety and dynamically determine the trajectory based on consideration of a small portion of the path ahead. This approach lends itself to situations in which the path may need frequent revision due to obstacle or road edge avoidance and it is expected future work will expand the algorithm to provide such intelligence.

Heading

Simple Steering Algorithm

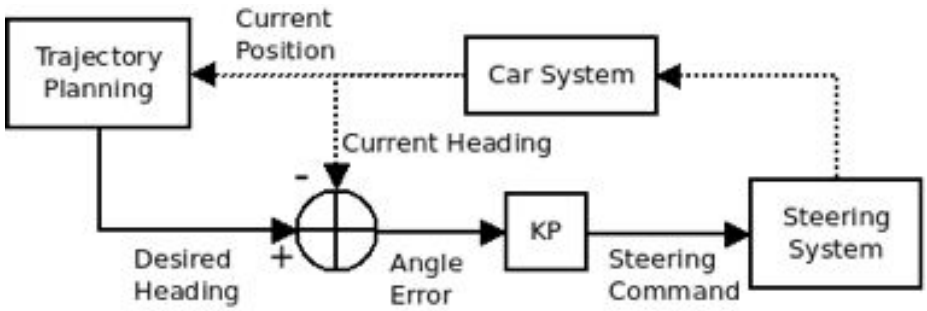

Figure 28: Steering control overview.

Initially, an extremely simple algorithm based on navigating in a direct line from the current position to the next waypoint in the map was implemented. The car's trajectory is calculated each time an updated position measurement is received and a vector from the current position to the next waypoint is established. The bearing associated with this vector is then calculated and used as the set point for the steering control loop, aiming to take the car on the shortest path to the next waypoint.

Measurement of the cars current heading (from the fusion algorithm) is compared with the heading required by the trajectory and a steering controller output computed in the traditional fashion of a feedback controller. The output to the drive-by-wire system effectively sets a

front-wheel steering angle and affects the current heading of the vehicle as well as its yaw-rate. The kinematic model for front-wheel steering of a vehicle under the assumptions of zero side-slip [50] gives the following definitions for the components of the course angle $\gamma = \psi + \beta$ (which is the heading referenced in standard position) as described in Figure 29:

$$\beta = \arctan\left(\frac{l_r \tan\delta_f}{l_f + l_r}\right) \quad , \quad \dot{\psi} = \frac{V\cos(\beta)}{l_f + l_r}\tan\delta_f$$

In these equations, the value β is termed the vehicle slip angle and ψ the yaw angle. In this implementation the controller gain, K_P, is set to the inverse of the slope derived from the calibration of the drive-by-wire controller, resulting in a 1-1 relationship between the heading error and the wheel angle δ_f. This results in the wheels pointing directly in the desired direction of travel at zero velocity, which is a slight underestimation given the non-linearity of the vehicle slip angle with the wheel angle. In dynamic operation the algorithm will reduce the steering angle (and hence yaw-rate) as the vehicle becomes aligned with the desired heading, a situation in which lower gain is beneficial given the physical limitations on the speed at which the wheels can be turned.

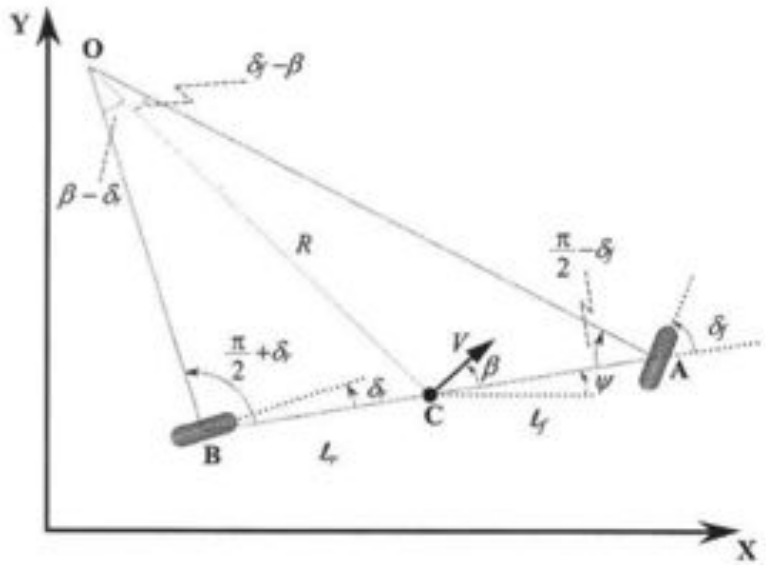

Figure 29: Kinematic model of lateral vehicle motion. Source: [50]

During testing it was found that the major shortcomings in this algorithm were related to the computation of the desired heading itself. In particular the lack of information about the future of the trajectory beyond the next waypoint led to a drastic change in desired heading each time a waypoint was met, resulting somewhat "jerky" steering action. Secondly, certain map arrangements resulted in the car arriving at a waypoint on an angle from which it was not physically possible to reach the next waypoint without having to drive around the waypoint and

attempt to reach it again. Lastly, it was identified that better path planning would enable the use of smaller waypoints which due to the size required in order to ensure stability in this algorithm led to "cut-corners" on the insides of curved sections.

Improved Steering Algorithm

An improved steering algorithm was implemented which is based upon interpolating a smooth path through the next several waypoints so as to achieve human-like driving and adds an element of "feed forward" control to the system. This was achieved by calculating cubic splines through the current position and the next three waypoints. The heading calculations thus lead to a path having continuous and equal first and second derivatives at each waypoint, causing the car to arrive at the next waypoint at an angle appropriate for continuing its journey to the following waypoint. The third order polynomial splines used are defined piece-wise, parametrically, between the cars current position, the first waypoint and each successive waypoint and possess the following properties (derived from [51]):

$$\vec{s}_i(t)=\begin{bmatrix} x \\ y \end{bmatrix}=\begin{bmatrix} a_i t^3+b_i t^2+c_i t+d_i \\ e_i t^3+f_i t^2+g_i t+h_i \end{bmatrix}$$

$$\vec{s}_1(t_0)=\vec{r} \quad , \quad \vec{s}_n(t_n)=\vec{w_{c+n}}$$

$$\vec{s_k}(t_k)=\vec{w_{c+k}}=\vec{s_{k+1}}(t_k) \quad \text{for} \quad k=1,\ldots,n-1 \quad .$$

$$\vec{s_k}'(t_k)=\vec{s_{k+1}}'(t_k) \quad \text{for} \quad k=1,\ldots,n-1$$

$$\vec{s_k}''(t_k)=\vec{s_{k+1}}''(t_k) \quad \text{for} \quad k=1,\ldots,n-1$$

$$\vec{s}_1''(t_0)=0 \quad , \quad \vec{s}_n''(t_n)=0$$

where $\vec{s}(t)$ is the spline interpolation, $\vec{r}$ is the current position vector, $\vec{w}_c$ is the position vector of the last reached waypoint and t is pseudo-time.

The splines are required to be fitted against time as in the case of a general map the y coordinate is not a function of x and because the motion of the vehicle is required to be smooth in time as well as in space. In order to achieve this, a "pseudo-time" scale was developed based upon the assumption of constant velocity between the waypoints. The distance in each segment in the spline is calculated as a straight line and used as the increment for the pseudo-time in to the next spline point. This method creates an estimated temporal spacing between the waypoints, allowing the interpolation to be carried out to give physically reasonable results. The first derivative at the beginning of the interpolated curve is then used to compute the desired heading with the interpolation recalculated in each cycle of the steering control loop.

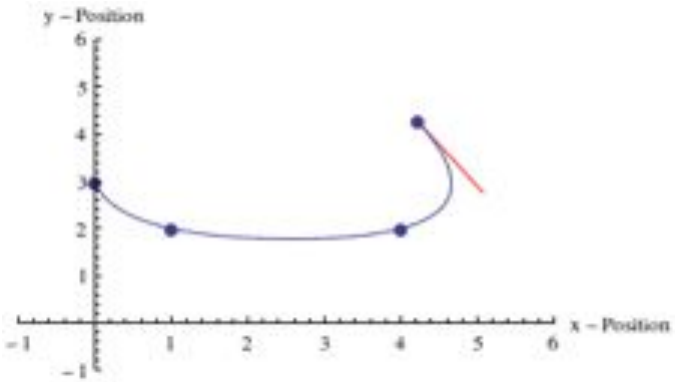

Figure 30: Interpolating three points ahead. The desired heading at this instant is shown in red.

Speed

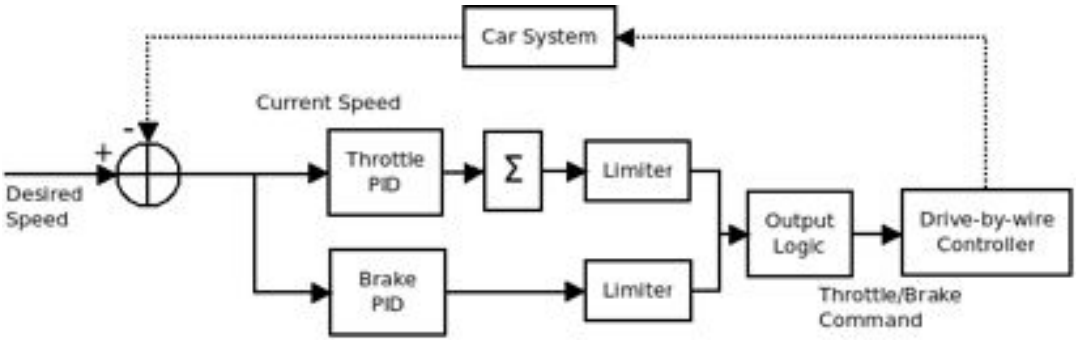

Figure 31: Speed controller overview.

The control program is able to instruct the drive-by-wire controller to operate either the brake or throttle at any one time. The value of the brake travel and throttle value required are computed by two separate PID controllers. This enables tuning of each action independently and is required given the nature of operation of the two functions. Braking occurs in response to a high-speed condition and the brake is operated only until the desired and actual speeds match. Manipulation of the throttle is incremental since the PID controller is required to converge on a non-zero throttle value, thus the PID output is summed with the current throttle set position to give the new set position at each step. Limiting functions then ensure that the values of both controllers do not exceed the allowed range before the exact output is determined based on the value of both controllers. In general braking only occurs when the throttle value has reached its bottom limit i.e. when the throttle controller has been unable to reduce the speed sufficiently quickly.

During testing the speed controller has been set to between 4 km/h and 10 km/h due to the necessity to severely limit the motor power for safety reasons whilst driving the car on-campus. In order to verify the operation of the controller, the speed set point was determined based on the steering radius, with the car travelling more slowly when cornering. It is intended that eventually

the desired speed would be calculated based upon the car's kinematics and the intended path so that appropriate speeds could be selected allowing the car to operate based upon its kinematic limits.

5.3 User Interfaces

The Autonomous SAE Car navigation controller can be interacted with in one of two ways – via the base station developed in this project or in a self-contained fashioned utilising and interface with car mounted LEDs and push buttons developed by Calvin Yapp. The product of these two modes of operation are three distinct interfaces – the choice of which to use depending on the level of functionality required. In the most basic case the Autonomous SAE Car can be operated with no external interaction, simply by pressing buttons located on the car's control panel. Further information and control functionality can be gained from the remote use of the web interface on any Wifi enabled device and lastly the base station hardware interface provides direct manual control and safety functionality essential for unmanned operation.

The interfaces designed in this project focus on achieving operational simplicity by providing functional tools which minimise the efforts of an operator whilst also providing a high degree of relevant feedback. Prior work at UWA has investigated the creation of interfaces for mobile robots with a map-centred interface and control panels providing commands with the overall goal of operating in a similar way to a “Real Time Strategy” video game [52]. In that project, a set of Interface Design Guidelines were defined and have been applied to this project where relevant. Research at Brigham Young University [53] has focussed on the development of a set of seven principles for creation of interfaces which are time efficient – defined by a minimisation of interaction time and a high degree of neglect tolerance. Neglect tolerance refers the systems ability to continue to perform its functions during periods of user neglect and is an essential concept in this project where interaction should be very limited. Ideally, the user would only need to interact with the Autonomous SAE Vehicle when starting the autonomous drive, after which the system should operate without human interaction at all.

Base Station Driven

Base Station Hardware Interface

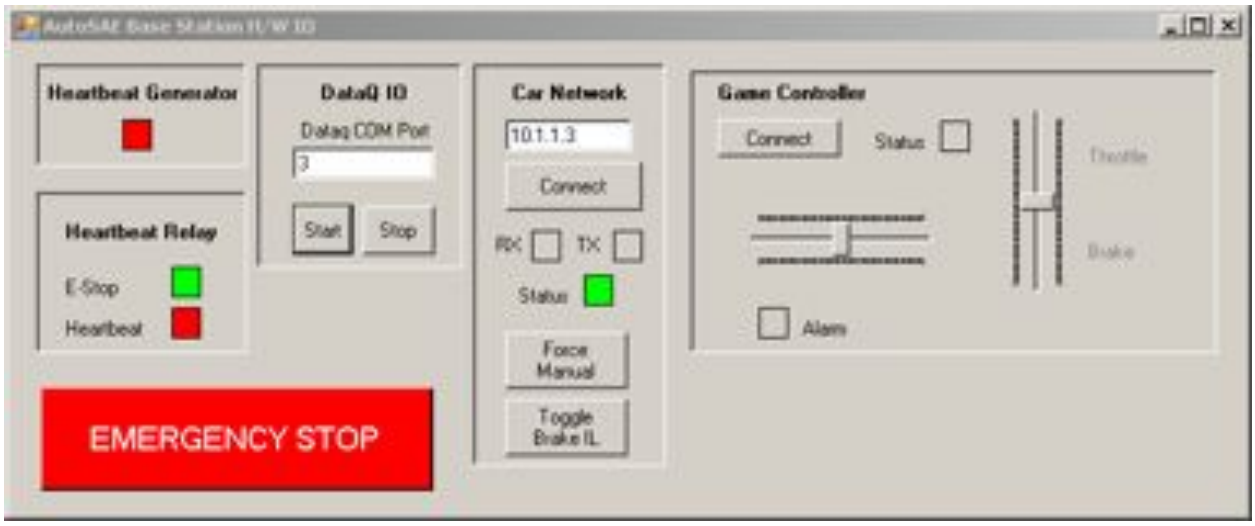

Figure 32: Base station control panel interface.

The base station hardware interface is designed for minimal human interaction and should ideally run in the background on the base station computer. The interface itself is broken up into five separate panels, each concerned with a separate system (e.g. input from USB button, output to car etc.). A series of coloured panels are used to give a visual indication of the status of operation, with red indicating a failure, green indication normal operation and grey indication that the system is not turned on. If manual control of the vehicle is desired – only interaction with this interface is required as use of the "Force Manual" button will override any other mode of operation allowing for an efficient transition to manual control with minimum operator effort. Once started and operation of this system verified, it may be "neglected" by the user during operation of the vehicle. Any system failures are accompanied by a pop-up message, which brings this interface back into the users scope of attention as per the principle of "attention management" identified in [53].

Web Interface

Traditionally robot interfaces have been developed using a variety of graphical toolkits to build stand-alone PC applications, some specifically designed for a particular robot system [52] and others which have been designed to be portable [54]. In this project a web-based interface was developed consisting of dynamic HTML pages delivered by a web server located on the Autonomous SAE Car itself. This approach has a number of benefits over traditional methods including reduced development time, familiar user interface paradigm, ease of access and platform independence. Earlier attempts at robot web interfaces implemented customised

software and focussed on the the applications in long-distance control of robot systems over the Internet [55] [56], however, more recent work has implemented interfaces based upon standardised AJAX/HTML [57] techniques for data display.

The interface implemented in this project is specific to the Autonomous SAE Car, but utilises standard software libraries and techniques, all of which are freely available and easily reused in other applications. The interface consists of three web pages (see Appendix D), the first of which is used for generating maps and control of the car. It is again split into functional control panels and features sections for recording maps by pointing and clicking on the Google Maps interface, tools for editing existing maps, a listing of the current status of various software parameters, buttons for sending commands to the vehicle and a display of the control system log. The use of Google Maps provides a familiar, easy to use, interactive interface, however, a display showing factors relating to the car's trajectory during autonomous driving was found to be more useful during execution of the map. This display shows the current position of the car in the local Cartesian coordinate system, the past and future waypoints on the trajectory and an indication of the car's actual and desired heading.

The concept of “externalizing memory” [53] has been implemented through two web pages which allow the replay of data captured during operation. The first displays a RADAR-style plot of the LIDAR data showing all four layers of scan data, the detected road edges and an overlay of any detected object regions. Live data is available for testing as well as the ability to view any previously detected data. Secondly, a web page dedicated to post-drive analysis provides eight different graphs displaying the behaviour of the trajectory generation algorithms, outputs to the drive-by-wire system and the cars velocity and path over the course of operation.

This web interface has performed very well during testing with the only practical limitation being the quality of the Wifi link to the vehicle, however, it should be noted that such a system is not appropriate for use in safety critical applications, hence the need for parallel implementation of the base station hardware interface. The interface design appears to have been time efficient during testing with around five clicks required to record and drive a mapped path. The potential for customisation and extension of this interface has proven very promising and represents an exciting opportunity for further improvement.

Self Contained Operation

An information only terminal interface was developed to provide a basic indication of the operation of the navigation controller it's various interfaces without having to refer to the base station computer. Use of the *ncurses* C++ library allows display of information with a consistent layout and allows for a degree of improvement over a simple scrolling terminal. The same IPC API offered by the navigation control program that provides communication with the web server has been utilised by Calvin Yapp in development of a self-contained interface which allows control of the system from a panel mounted on the vehicle. This system is based around a second, independent program and highlights the flexibility offered by this API for communication with a variety of interfaces and systems.

Figure 33: Control panel for safety system and car based interface.

6 Safety

6.1 Requirements and Design

Risk Assessment

Analysis and identification of risks and design of safety controls was considered as an integral part of this project due to the hazards associated with autonomous vehicles. Safety standards and design and verification methodologies for safety related systems [58] are well established for use in safety-critical systems in industry, however, these systems traditionally do not have the added complexity of human-robot interaction [59]. Research conducted as part of the Safety-SAM project [60] identified that system development can be broken into six major stages:

1. Safety analysis
2. Production of a safety requirements specification
3. Hazard partitioning
4. Specification of information requirements of the safety manager
5. System architecture design
6. Prototype development

Safety analysis involves identification of potential hazards and classification of the associated risks which can then be used to form a set of safety requirements. The hazards are then grouped together in terms of the systems that will be used to mitigate them allowing specification, design and implementation of safety systems to take place. An independent safety management system is typically implemented in order to achieve the safety requirements with a high reliability [59] [60].

Identification of hazards associated with the Autonomous SAE Car was based on the scenario of testing speed limited autonomous driving in an open area with members of the public nearby, however, the system requirements were created with operation at higher speeds in the future in mind. A variety of techniques exist for hazard identification including the chemical/process oriented HAZOP technique, SHARD (a variation designed for analysis of software) [59] and CLASH (a methodology designed for large autonomous vehicles) [60]. In this project, a team based brainstorming session was undertaken to identify hazards in a similar way to [59] and the results and requirements were recorded using UWA's risk-register template (see Appendix E). This analysis revealed that the most important consideration was the ability to detect failure of control and stop the car and hence the safety systems were designed in a way which seeks to maximise the reliability of this functionality.

System Design

The safety system implemented in this project is partitioned into functionality located in four logic solvers; the navigation controller, hardware safety supervisor, analogue driver safety module and the drive-by-wire controller (see Figure 34). The latter two are both considered components of the low-level system and are not discussed in detail here, however, they are interconnected with the high level safety systems and provide essential functionality. The analogue driver safety module is designed to detect attempts by a safety driver to override the drive-by-wire system via the steering wheel and brake pedal and reports such attempts to the safety supervisor. The safety supervisor provides an interface for the navigation controller to provide safety functionality as well as providing redundancy for critical functions and several auxiliary features. The drive-by-wire controller has it's own built in fault detection and is able to take action in addition to reporting faults to the navigation controller. It also provides an input, the “brake interlock” which is hard-wired (active low) from the safety supervisor and provides a means for requesting emergency braking in the case of failure of the navigation system or power loss in the safety supervisor.

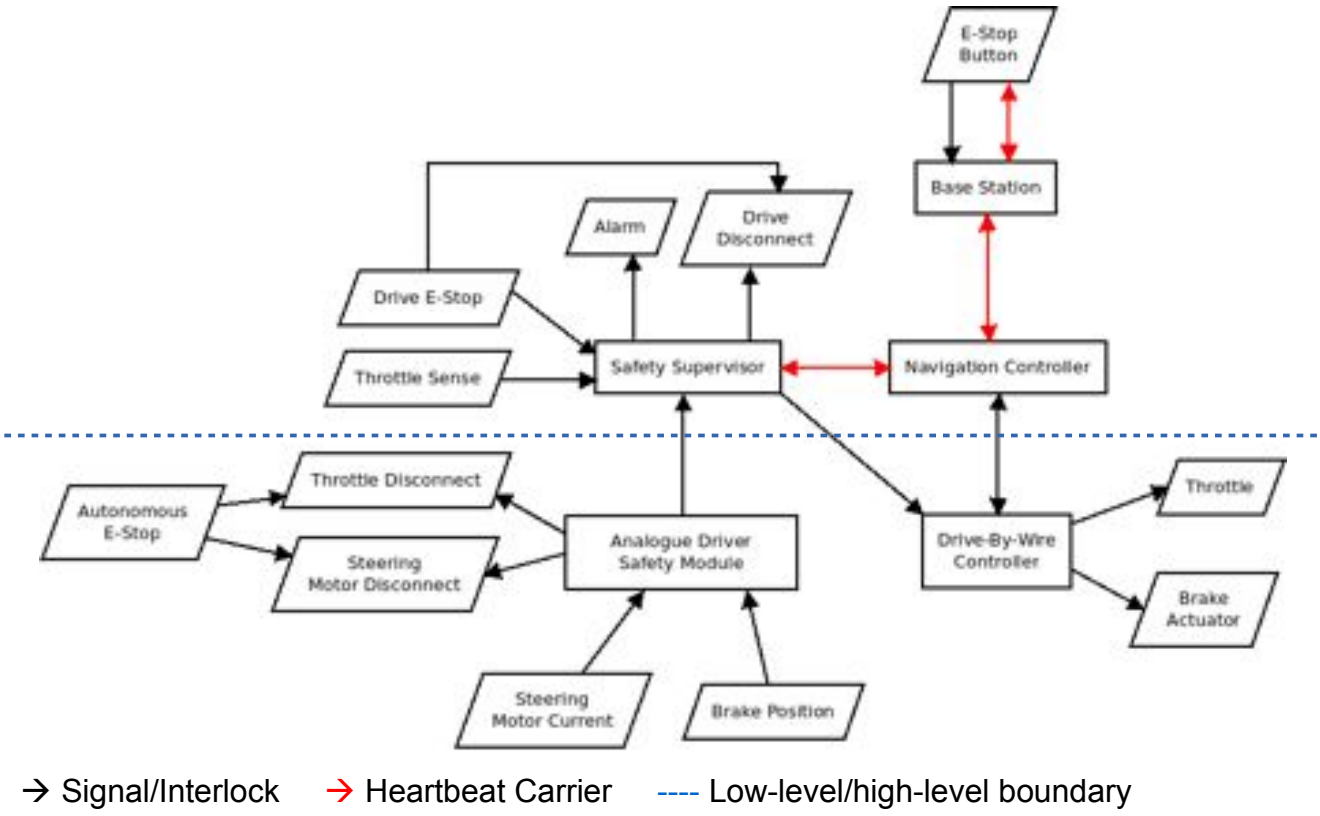

Figure 34: Safety system relationship diagram.

The design for the safety system was based upon two distinct profiles of operation – the first in which a "safety driver" is present in the vehicle and is able to take action in the case of a loss of control and the second in which the car drives fully autonomously with no person present. In the first instance, the ability to remotely stop the car is desirable, but not strictly necessary and so two safety modes were developed in order to allow more flexibility during operation (e.g. driving where Wifi is not practical). Thus, in the human driving profile, a trip will not be initiated when connection between the base station and car is interrupted and autonomous driving will be able to commence without an active Wifi connection.

In the fully autonomous profile the "heartbeat" signal which originates at the base station and terminates at the hardware safety supervisor is required to be present. This signal is a 10Hz binary square wave sampled at 50Hz via the base emergency stop button (see section 3.2) and transmitted via the TCP/IP over Wifi link to the navigation controller. The navigation controller then passes the signal onto the safety supervisor over the serial connection as well as performing verification that the network connection is error free. The safety supervisor measures the time between heartbeat signals and is able to initiate an emergency stop if the time period exceeds the set value. As the emergency stop button, base station, Wifi link, navigation controller and serial connection must all be functioning for this signal to be transmitted in a timely fashion the system is fail safe and provides protection against a variety of failure scenarios.

6.2 Integrated Safety Features

The navigation controller features integrated error detection and will enter a trip state if any thread calls the *Control::Trip()* function. After entering a trip state the navigation controller will disable autonomous driving, set the accelerator value to zero and send an emergency stop command to the hardware safety supervisor. Each call to *Trip()* must be accompanied by a reason number, which identifies the error message to be recorded in the log to aid diagnosis of faults (see Table 8 below). The base-station likewise incorporates integrated fault detection and will automatically send an emergency stop command if the connection to the USB controller fails while the heartbeat loop through the emergency stop button ensures that failure of the stop button interface is detected.

№	Reason
1	Base ESTOP
2	Couldn't send HB
3	Safety supervisor initiated trip.
4	Safety supervisor msgs not ack'd.
5	Error sending low level commands.
6	Network error!
7	GPS Error
8	Autonomous issue
9	Web IPC estop
10	Low Level Error

Table 8: Navigation controller trip codes.

Both the hardware safety supervisor and drive-by-wire controller provide acknowledgement and informational messages back to the navigation controller, the latter of which are recorded into the log file for diagnostic purposes. The *SafetySerial* class provides verification that the correct acknowledgement has been received in a timely fashion so that any error in communication or hardware fault can be detected whilst the *LowLevelSerial* which deals with substantially more data simply ensures that at least one acknowledgement is received within 300ms, facilitating detection of a failure in the drive-by-wire controller or the associated communication link. *LowLevelSerial* also receives and parses error codes (see Appendix B) sent by the drive-by-wire controller which are logged and, if required, a trip initiated. As accurate positioning data is essential to the autonomous vehicle's safety, a check is made of the age of the GPS fix every half a second. If the time value reported by the GPS module has not increased by 100ms at each check, the GPS fix is deemed to be old and the car will enter a trip state.

The TCP/IP connection implemented between the navigation controller and base station in the *CarNetwork* class incorporates error checking including detection of the lack of a message after one second, disconnection mid-message, detection of empty messages and an inability to write to the socket. Any issues detected with the network connection result in a log entry and a trip state will be entered if the car is currently in the fully autonomous safety profile. Measurement of the heartbeat interval is also undertaken and a log entry is made when the interval exceeds 100ms for use in diagnosis of problems with the heartbeat relay.

6.3 Hardware Safety Supervisor

The hardware safety supervisor system was created in order to add a level of redundancy to the car's safety systems. By implementing the system as a self-contained device additional risk-reduction is achieved compared to integration with the high or low level primary control systems and is implemented to passively monitor the control systems, human inputs and to perform independent actions in the event of a trip initiator. The following design specification was created in order to summarise the required functionality:

Function	*Importance*
Monitor the heartbeat from the high level control system.	High
Disconnect drive power in trip condition	High
Implement an “arming sequence” and prevent the throttle from activating soon after the drive is enabled	Medium
Apply the brake via a hard-wired signal to the low level controller	Medium
Provide audible notification of a fault	Medium
Provide feedback as to the state of trip systems	Medium
Allow high level control actions based on low-level safety systems	Low
Require physical intervention when restarting systems after a fault	Low

Table 9: Hardware safety supervisor design requirements.

It was also identified that automatic full-lock braking is inappropriate when the car is in the “safety driver” profile. In the case of a failure or unexpected event, heavy braking is always the first response, however a human is able to judge the extent to which this is appropriate in maintaining stability and coming to a safe stop in an appropriate position. Therefore the system should cut power to the drive system and relinquish braking and steering to safety to the safety driver. Thus, an additional desirable criteria is for the hardware safety supervisor to have awareness of the high level control systems safety profile and to act based on this knowledge.

Hardware

Two possible design solutions were considered for the hardware safety supervisor. An implementation consisting of only discrete electronic components was initially considered based upon a missing-pulse detection circuit for monitoring of the heartbeat and an analogue timer circuit for implementation of an arming sequence. However, despite its increased integrity, such an approach offers extremely low flexibility and does not scale well. Due to the time required to develop and test such a system as well as the size of the hardware required in order to implement all of the functionality discussed above it was decided to consider a micro-controller based solution instead.

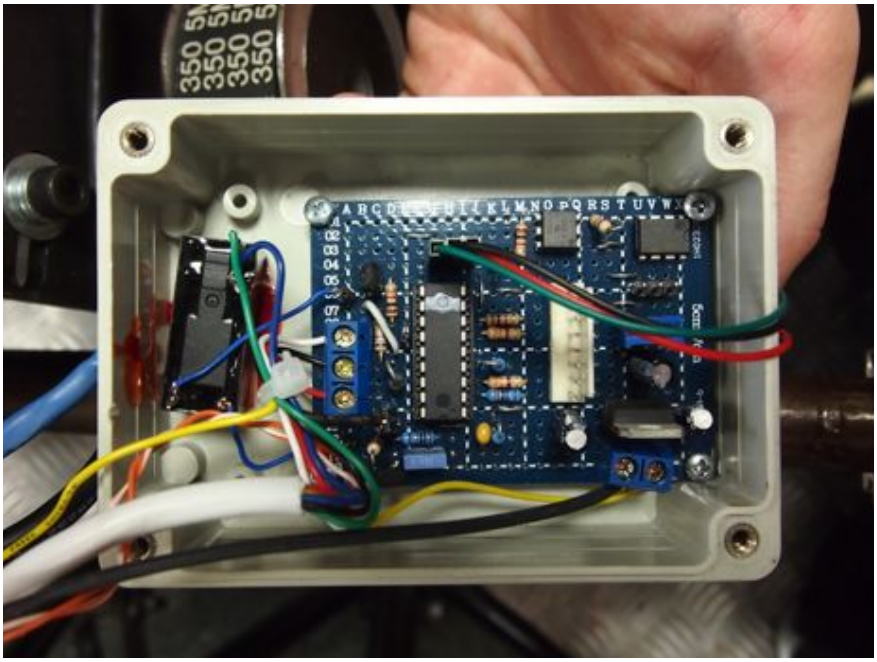

Figure 35: Constructed hardware safety supervisor.

The system design is based around the PIC16F88, an 8-bit micro-controller from Microchip. This device was selected for its built-in hardware UART, small DIP-18 package, ability to source 25mA from an IO pin, built in oscillator and ease of programming [61]. As a result of these features the circuit was able to be constructed using through-hole techniques on a 7x5cm PCB and only two additional ICs were required in addition to the PIC. The PIC16F88 also features a hardware watchdog timer module which acts to supervise the operation of the safety supervisor itself by resetting the micro-controller if the timer expires. In this application the *WDTCON* register has been set to give a period of 16.38ms and the *CLRWDT* instruction is issued to reset the timer at the start of every loop in the running software. Thus, the controller is protected against any scenario in which the software ceases to continue executing.

The circuit (see Appendix F) derives its power from the autonomous/manual switch located on the safety control panel. The NO contacts are used to supply power to the low-level controller as well as to the hardware safety supervisor via a LM7805 three terminal voltage regulator which provides a clean 5V supply to the micro-controller. The NC contacts provide 12V directly to the base of Q1 so that K1 is closed and the drive can be enabled when the car is in manual mode. The silicon signal diode D1 protects the micro-controller IO from the applied voltage in this scenario. Relay K1 is powered directly from the always-on 12V supply and LED5 provides visual indication of its position. K1's NO contacts are connected in series with the existing dash-mounted emergency stop button and the loop is connected to the drive enable inputs on the BMS pre-charge circuit which powers the drive system. A 12V flashing LED strobe light was

installed in parallel with the main drive contractor's coil and mounted on top of the car as per current Formula-SAE regulations giving an indication of the actual drive status from afar. An additional bipolar transistor, Q2 drives a piezoelectric transducer which provides a 80dB SPL alert tone which is activated during trip conditions or remotely as a horn. As the PIC16F88 is able to source up to 25mA per IO pin, indicator LEDs showing the heartbeat activity, trip condition, throttle timer condition and safety system profile are able to be driven directly via current limiting resistors.

The PIC16F88 features an internal oscillator block and in this case it has been configured to run at 8MHz – it is factory tuned and is typically accurate to ±1% at room temperature, which is quite sufficient for this application. The hardware safety supervisor receives input from the high level control system via an inexpensive USB-serial converter module based on the PL2303 IC. This interface is supported natively under Linux and provides a TTL level interface compatible with the micro-controller's UART. In this instance the serial communication is implemented at 38400 Baud as this rate is able to be implemented with minimal error utilising the PIC's internal oscillator;

$$Baud\ Rate = \frac{F_{OSC}}{16(X+1)} = \frac{8*10^6}{16(12+1)} = 38461.5 \quad [61]$$

where X is the value written to *SPBRG* register which configures the serial port.

Extensive use is made of the PIC's built in timer module, TMR0 for checking the period between heartbeat transitions as well as implementing delays in the arming sequence. The PIC's *OPTION_REG* register has been configured so that the timer is interrupted by a signal prescaled by dividing the instruction clock by 256. The *TMR0* counter register is then preset to 100, resulting in the register overflowing and triggering with frequency:

$$F_{interupt} = \frac{8*10^6/4}{256*(256-100)} = 50.08\,Hz$$

Thus, timing operations are easily implemented by counting the number of interrupts required for a desired time interval.

Additional IO is handled using the PICs two IO banks, with bit numbers selected based on the circuit board layout. Inputs from switch contacts are in a pull-up configuration and switch de-bouncing is handled in software whilst the normally-high brake interlock output to the low-level controller is pulled down and loaded with a small capacitor in order to provide a fail-safe scenario and increase noise immunity respectively. Input from the throttle line to the

Kelly motor controllers is applied to an LM358 op-amp configured as a comparator and compared against an adjustable reference. The output of this is provided to the micro-controller via an optoisolator as the throttle signal is referenced to the drive train power supply.

Software State Machine

The micro-controller software was developed using MikroElektronika's ANSI C PIC Compiler suite and takes the basis of a state-machine design. The software accomplishes four primary functions; monitoring the heartbeat signal, acting upon trips initiated by the navigation controller, reporting trips initiated by the analogue hardware safety module and allowing for safe "arming" of the autonomous system. The micro-controller continuously receives commands consisting of a single ASCII character (see Table 10) from the navigation controller via its UART and sends reply messages consisting on a variable length string followed by the new-line character.

Command	***Description***
E	Emergency stop
+	Heartbeat high value
-	Heartbeat low value
B	Set brake interlock on (fully autonomous safety profile)
H	Set brake interlock off (human safety driver profile)
A	Sound piezo alarm

Table 10: Hardware Safety Supervisor Command Set

The arming sequence is designed to mitigate the risk associated with the possibility of the car accelerating due to hardware or software failure in the time period immediately following enabling the drive system. A sequenced start-up has been implemented which operates as follows:

1. Operator holds arm button
2. Full brake is applied
3. After 4s the drive system is enabled and throttle sensor turned on.
4. After a further 4s the operator can release the arm button – any premature release will disconnect the drive.
5. After 10s the brake releases.
6. After a further 2s the throttle sensor is disabled.

This means that the arm button must be held for a total of 8s for the drive to stay enabled and protects against accidental start-up. The 4s delay after the drive is enabled before latching provides the operator an opportunity to disconnect the drive power simply by letting go of the button if something goes wrong immediately after the drive is enabled. If a throttle voltage is detected within 16s of the drive being enabled the drive will also be disabled giving the operator time to move away from the car before it is possible for it to start moving. A lack of heartbeat signal or trip condition initiated by the navigation controller, analogue driver safety module or dash emergency stop will result in the drive being disabled and alarm activated.

The implementation of this functionality consists of a set of states with associated outputs and transition conditions, with the identity of the current state contained in an integer variable (see Appendices G and H for the state diagram and output table). The program's main loop consists of receiving input from the UART and performing any actions required based upon it (such as resetting the heartbeat timer), followed by evaluating the conditions required for transition from the current state into another. Extensive informational messages are relayed to the navigation system during arming and when a fault is detected as well as acknowledgement responses for each command received over the serial link.

This system has performed well and required minimal adjustment, however, the maximum allowed interval between heartbeat transitions had to be increased beyond the desired 200ms (chosen to give a maximum travel of around 3m before stopping at 50km/h) in order to achieve stable operation. It was found that whilst the safety supervisor was capable of this interval the Wifi connection to the base-station was not able to meet this specification reliably and as a result the interval was increased to 600ms. The cause of this issue is mostly likely interference from other 2.4GHz networks at UWA as the Wifi transceivers used are designed to work at the distances involved in this project. This has not caused an issue as testing has been carried out at speeds significantly lower than 50km/h, however in the future this issue will need further examination.

7 Results

Testing of the Autonomous SAE Car took place on the Chemistry lawn, located on campus at UWA. This location offered convenience, however, due to the size, hazards present at edges of the area and the significant pedestrian traffic around this area, the car's power was significantly reduced and the scope of testing limited to relatively simple patterns. A substantial amount of data was collected via logging during testing of the car as well as via specific experiments and the strengths of the system, as well as areas that require further attention in this implementation have been identified.

7.1 Position & Heading

Testing of the heading fusion algorithm was performed in order to ensure correct operation under dynamic turning conditions as well as to ensure absolute accuracy in a straight-line situation. Figure 36 shows the operation of the heading fusion algorithm during an autonomous drive and highlights the GPS module's shortcomings in reporting a heading. From 0 seconds until approximately 40 seconds, the GPS unit has reported a completely erroneous track angle due to the car moving at a very low speed. Following this point, it can be seen that the GPS and IMU are in relatively close agreement, however there are periods of excessive noise in the GPS heading. It is therefore pleasing to note that the heading fusion algorithm has operated as expected.

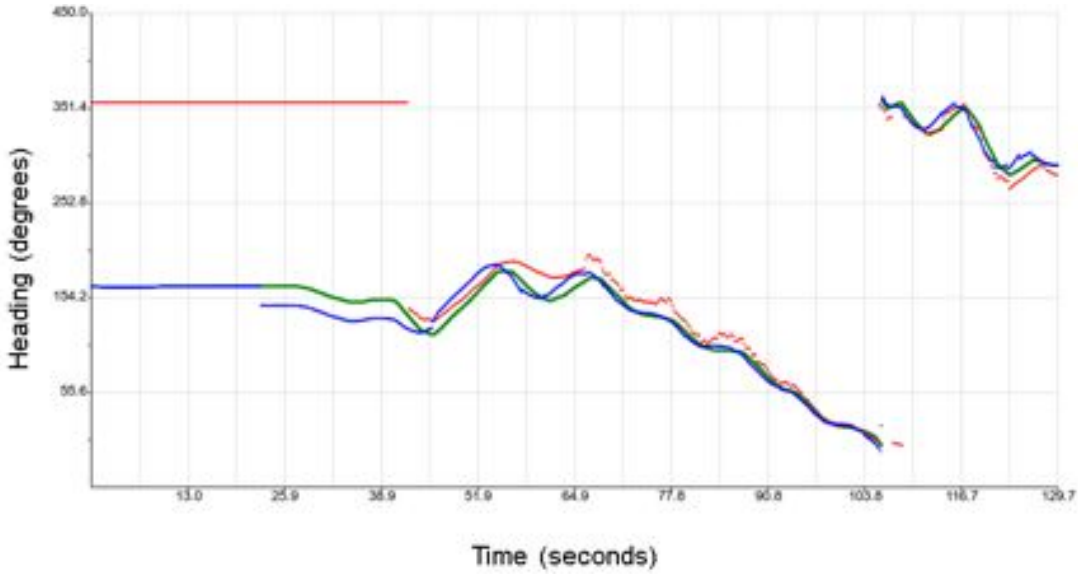

Figure 36: Example of heading fusion during driving (red – GPS, green – IMU, blue - fused).

In order to evaluate the absolute accuracy of the heading fusion algorithm and the operation of the position filtering algorithm a closed loop consisting of a straight line driven from North to South and a similar South-North section were driven manually. The line to be followed was marked on the ground and its direction checked with a map and magnetic compass. The heading measurements shown on the right of Figure 37 show that the bearing reported by the car's sensors was accurate, with 180º and 0/360º measured for the two sections. Evidence of the GPS modules noise, poor resolution and limited accuracy at the start/end of the driving section were also observed in this experiment.

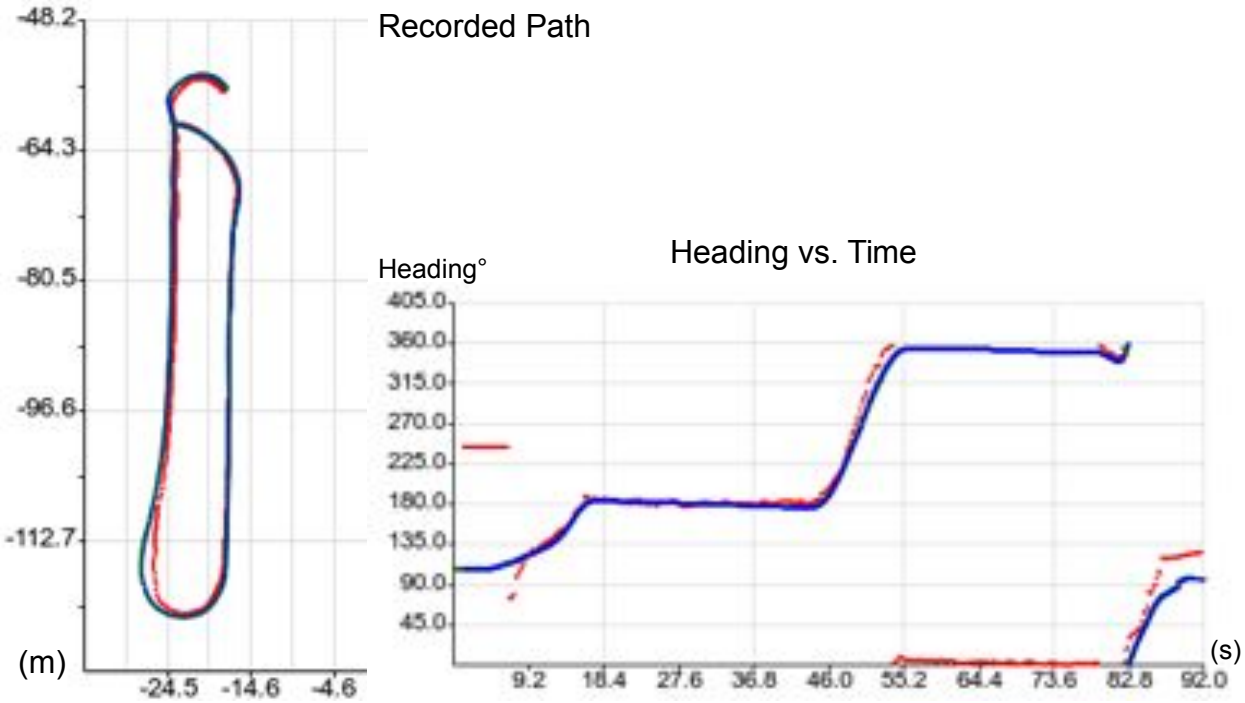

Figure 37: North-South loop position and heading (red – GPS, blue – fused).

This experiment also reveals the effectiveness of the position filtering algorithm, particularly when expanded in scale as shown in Figure 38. The GPS position resolution and update rate are somewhat limited, whilst the fused position is substantially more smooth and masks the GPS modules shortcomings. The GPS data around the South-North turn in this test drive shows a deviation of approximately two metres as well as increased noise, however, the filtered position in this region is again smooth and more importantly physically consistent with the pattern being driven in the turn. It is therefore evident from this data that the filtering algorithm is of benefit.

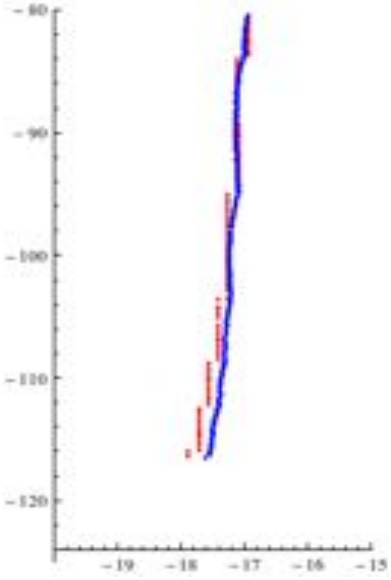

Figure 38: Straight line section expanded scale (position – metres).

7.2 Road Edge Detection

In addition to the static proof-of-concept testing shown already displayed, three trials were run in order to measure the success of the algorithm in dynamic scenarios. In all three cases, the car was driven down a section of road of fixed width, at an approximately constant speed and the road edges detected at approximately 4 Hz. The absolute accuracy of the algorithm can thus be inferred from the measured width of the road, a measurement which can be considered to be the sum of two random variables $Z = X + Y$, denoting the left and right edge positions respectively. As it is extremely difficult to ensure constant alignment of the car laterally during driving these variables are not independent. However, the standard results for combination of Gaussian random variables can be used to infer the variance in the determination of each edge position by measurement of Z and assumption that X and Y were, in fact, independent. Thus:

If $Z \sim N(\mu_X + \mu_Y, \sigma_X^2 + \sigma_Y^2)$ where $X \sim N(\mu_X, \sigma_X^2)$, $Y \sim N(\mu_Y, \sigma_Y^2)$

then $\sigma_Z^2 = \sigma_X^2 + \sigma_Y^2$.

Now, assuming that X and Y are independent and identically distributed and we have:

$$\sigma_X^2 = \sigma_Y^2 = \frac{\sigma_Z^2}{2}.$$

These result is not surprising and hence an estimate of the error in determining an individual edge edge can be estimated from the road-width measurements. A similar argument allows us to estimate the difference between the mean of the observed and independently measured data, e.g.

$$\Delta\mu_X = \Delta\mu_X = \frac{\Delta\mu_Z}{2}.$$

Scenario 1 – Curb Detection on an Asphalt Road

Figure 39: Road section used in testing.

In this trial, the car was driven in a straight line along a curbed asphalt road as shown in Figure 39. The edges of this road were therefore linear in time up until around 60s at which point the

right hand curb curved off to the right. Figure 40 shows the detected road edges in raw form generated by the simple peak detection algorithm as well as the assisted identification of more appropriate edges with the four mode classification algorithm and finally the Kalman filtered road edge position. The algorithms were configured with a maximum allowed slope of 0.4 and allowed variation of 1.5m.

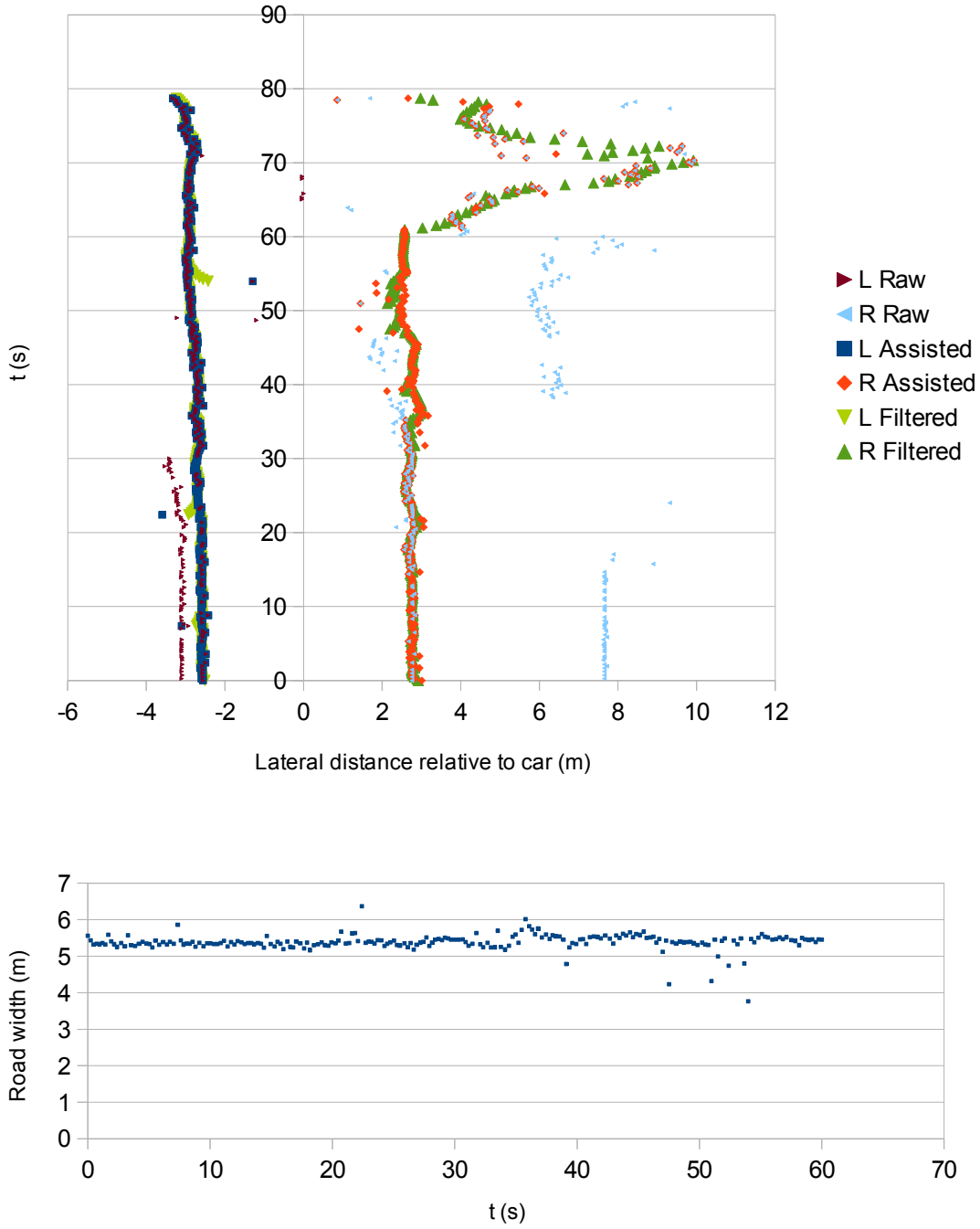

Figure 40: Road edge positions (top) and measured width (bottom) over time for a drive along a curbed asphalt road.

It was found that the average road width was 5.39m with a standard deviation of 0.23m. The road edge was measured manually in four locations and found to have an average width of 5.59m with a standard deviation of 0.01m. The slightly conservative (3.5% low) estimate for the width is most likely due to the presence of leaf matter and the slight taper present at the edge of the asphalt. The estimated standard deviation of an individual edge is 0.16m and thus in this scenario the edge has been identified with an accuracy of approximately 0.10±0.16m which certainly meets the stated performance requirement of 0.5m accuracy at each side.

Scenario 2 – Grass Edge Detection on a Paved Road

Figure 41: Paved pathway used during testing.

This test is was performed by driving the car down a section of brick paved road with grassed edges as shown in Figure 41. The path was not perfectly straight and due to the lack of clearly defined edge features less accuracy is expected. As a result, the algorithms were configured with a maximum allowed slope of 0.15m and an allowed variation of 1m. Results showing the edge position and measured path width are shown in Figure 42 overleaf.

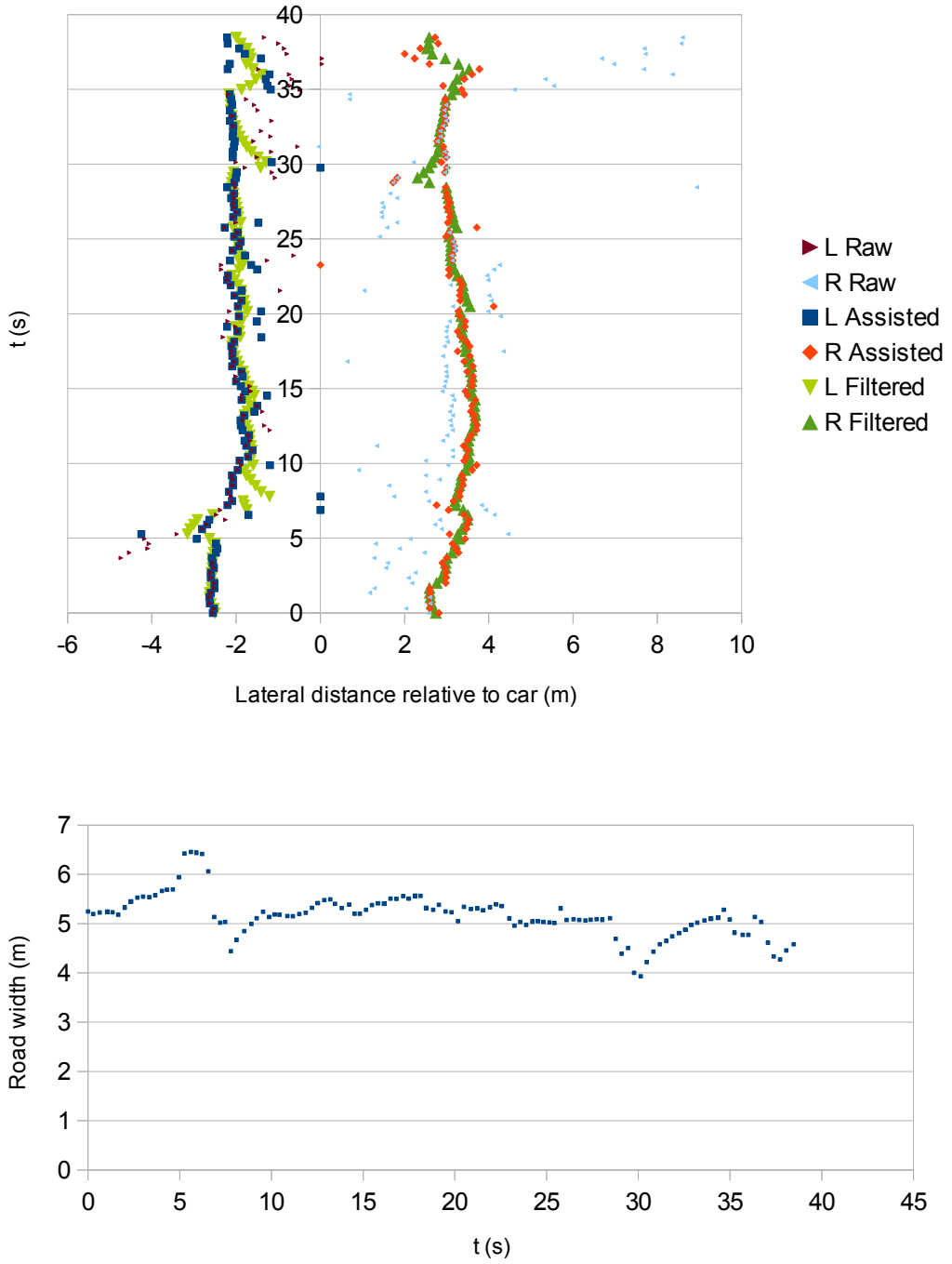

Figure 42: Road edge positions (top) and measured width (bottom) over time for a drive along a paved road with grass edges.

It was found that the average road width was 5.16m with a standard deviation of 0.44m. The road edge was measured manually in three locations and was found to consistently measure 5.05m, giving an average error of 2.2%. The estimated standard deviation of an individual edge is 0.31m and thus in this scenario the edge has been identified with an accuracy of approximately 0.06±0.31m which also meets the stated performance requirement of 0.5m accuracy at each side.

Scenario 3 – Curb Detection with Lateral Motion

In this scenario the car was driven along the same road segment as in Scenario 1 above, however the car was in a "wavy" pattern to simulate conditions under which the road edge position would be constantly changing. For this trial the maximum slope was set at 0.5 and allowed variation at 1.5m.

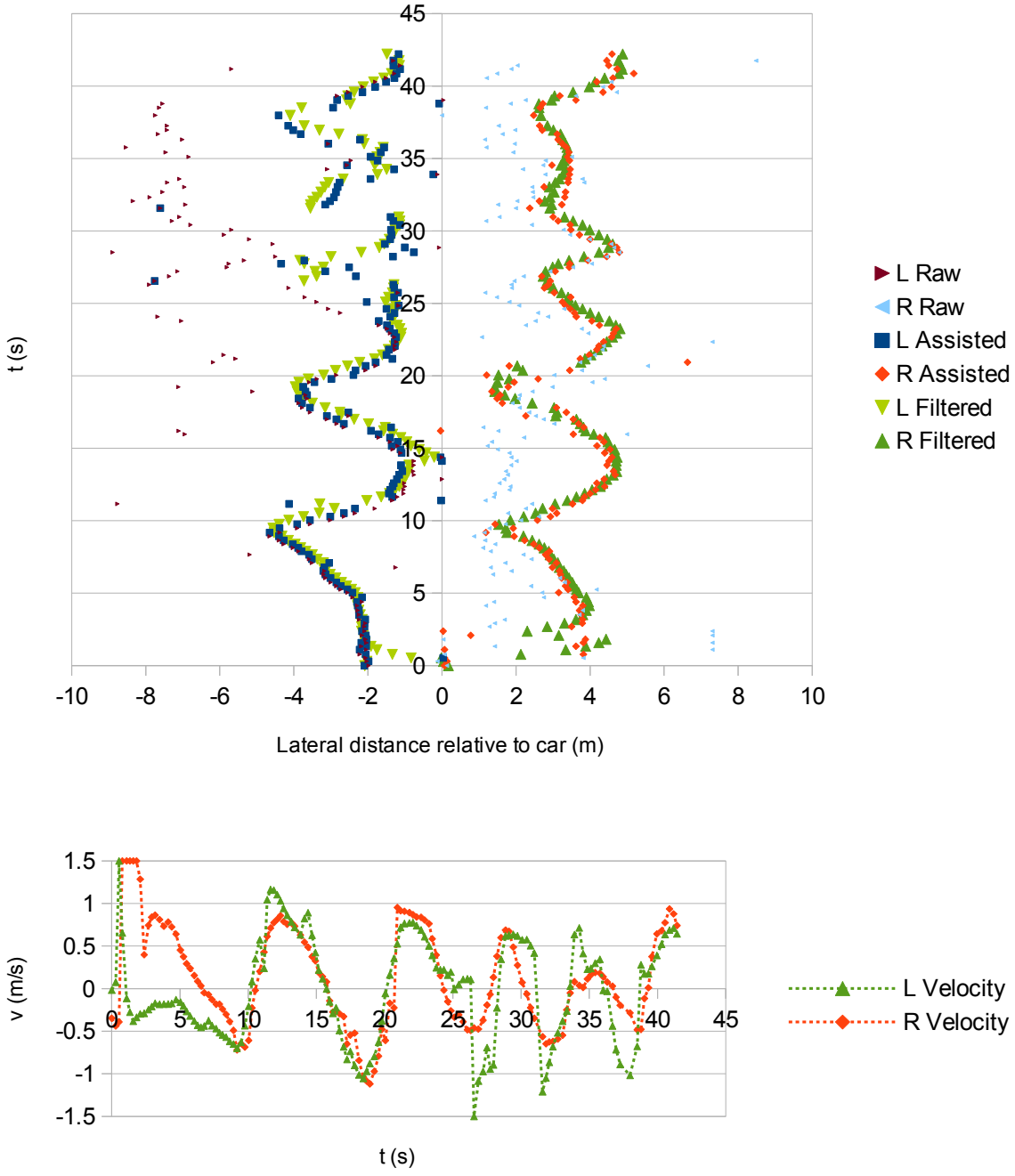

Figure 43: Road edge position (top) and edge velocity (bottom) on a curbed road with lateral motion.

Due to the constantly changing angle between the car and the road in this test it is not appropriate to draw conclusions from measurement of the road width, however it can be seen qualitatively the the algorithm has performed well and is able to track the road edges under dynamic conditions.

Performance of Edge Finding Modes

It was observed that the simple greatest local maximum peak detection mode was used in the majority of cases in scenarios 1 and 2, with the greater number of favoured dips in scenario 2 most likely due to the different edge characteristic. Pleasingly very few failures were experienced overall, however a large proportion of detected edges in scenario 3 required were identified via the reallocation mode, suggesting that the edges were often not evident without assistance in this scenario. This result supports the need for implementation of temporal filtering in this application as it has evidently improved the edge detection rate very substantially in this project.

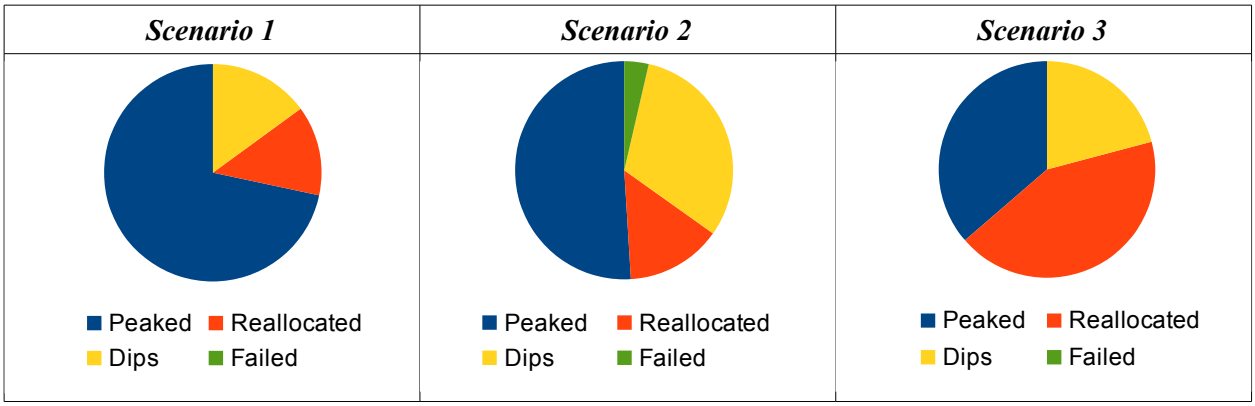

Figure 44: Proportional frequency of edge identification modes.

7.3 Autonomous Driving

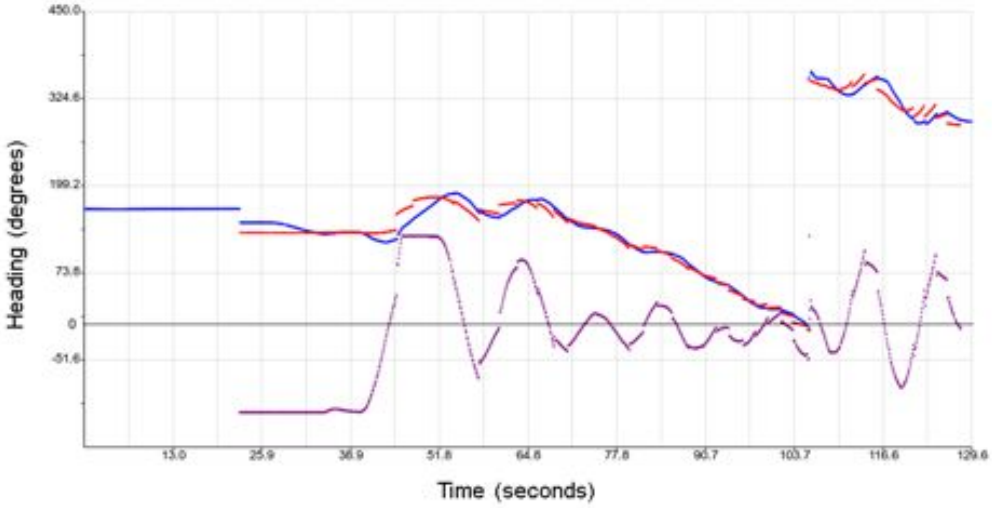

Figure 45: Operation of the trajectory control system during an autonomous drive (blue – car's heading, red – desired heading, purple – steering command value).

Operation of the steering control system during an autonomous drive is shown in Figure 45. The algorithm functions as expected, however it was noted that as successive waypoints were reached there was a significant change in desired heading, leading to steering correction. It was found that the average error between the desired heading and the car's actual heading was 14º which is somewhat larger than is desirable and it is clear that further attention is required to both trajectory planning and steering control.

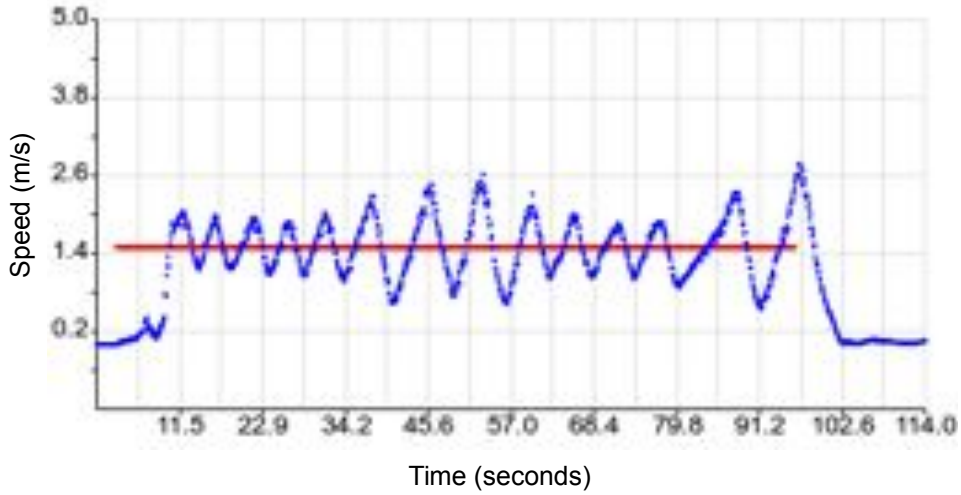

Figure 46: Speed control at low speed/power (red – set point, blue – car's speed).

Due the necessity of reducing the car's power so substantially for testing on campus, the speed control system was not able to be fully tested. It was observed that at low speeds some oscillation resulted due to the significant time-lag introduced into the control system as a result of the lack of available torque even when already moving. It is expected that with increased torque and better tuning this control system will operate in the required fashion.

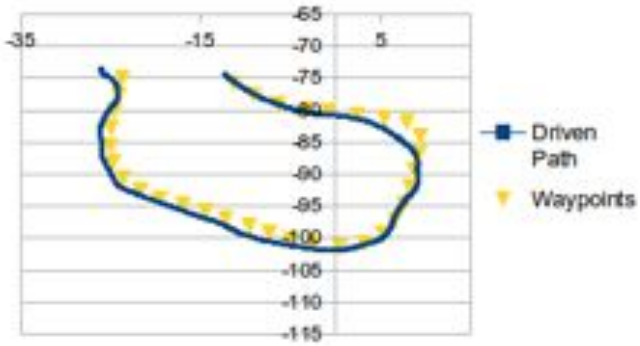

Figure 47: Comparison of driven path and the waypoint map (scale – metres).

Testing of the total system yielded pleasing results which were quite within the performance limits required for operation in a track scenario. Figure 47 shows a map and the position measured during autonomous driving with 2.5m radius waypoints. The mean closest-approach distance from the path to each waypoint was found to be 80cm with the best result being 10cm. In this particular trial it was found that the large size of the waypoints actually had a slightly detrimental effect on the measured results as it allows the car to "cut corners" whilst moving around the path. It is anticipated that even better results will be able to be achieved with smaller waypoints in the future.

Figure 48: Line video test setup.

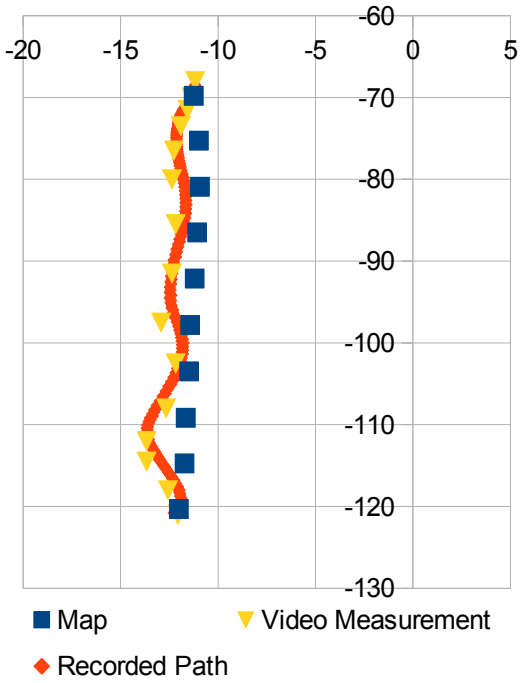

Figure 49: Line test results.

In order to determine the accuracy of the system referenced to the ground and to investigate which component of the system could most benefit from future work, a test was conducted in

which the car autonomously drove along a pre-recorded straight line. The car's lateral position relative to the line was measured via video analysis and plotted alongside the path measured by the car's sensors and the waypoints that made up the map. It was found that the trajectory measured independently using the video agreed well with the path measured by the car, providing evidence for the accuracy of the sensor fusion algorithm in an absolute sense. The lateral error observed had a mean of 70cm over the course of the drive and provides further evidence of the accuracy limits observed in the trajectory/steering control scheme. Despite this, the test does meet the performance requirements with regards to operation in a track scenario.

The final experiment performed was designed to test the operation of the improved trajectory generation scheme. A map consisting of only five waypoints with large distance separation was created in order to exemplify the effect, and was driven autonomously using both algorithms (see Figure 50). The most significant result of this trial was that the interpolated algorithm successfully resulted in the car arriving at each waypoint facing in a direction which allowed a smooth drive to the next waypoint rather than the sharp corners seen with the simple algorithm. As discussed in section 5.2 this is important for stability of the trajectory generation algorithm, evidence of which has recently been observed whilst testing more complex maps as well as for smooth, safe operation at greater speeds.

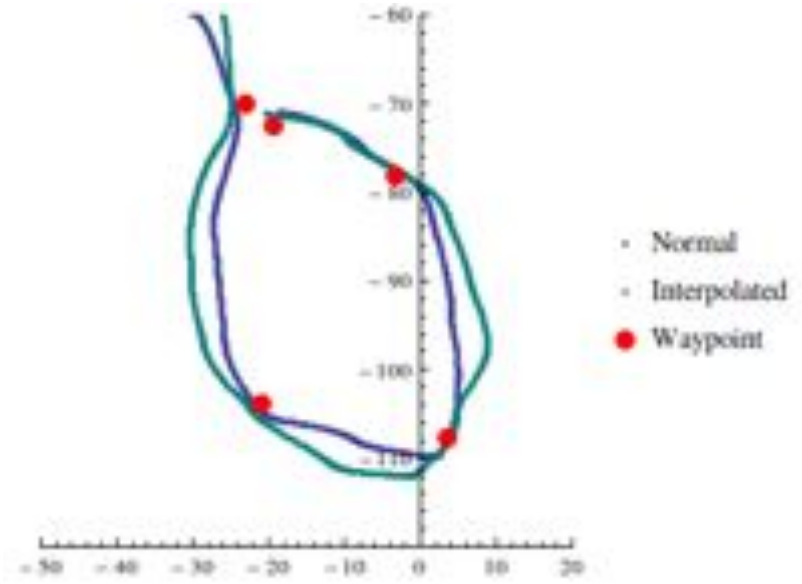

Figure 50: Comparison of simple and interpolating algorithms for a four waypoint map (scale – metres).

8 Conclusion and Future Work

Conclusion

This project shows significant promise as a platform for the development of autonomous driving technology and it is anticipated that with development of the underlying systems completed future work will focus on refining and improving the methods presented here. The project has achieved its goal of creating an operational and fully featured control system which allows the Autonomous SAE Car to drive maps with accuracy and safety appropriate for future testing on a race track.

The modular design of the software provides the ability to easily modify or implement new functionality and the hardware systems installed on the vehicle have proven robust. The sensor array implemented successfully provides sufficient information of a quality useful for driving in a variety of scenarios. In particular, the sensor fusion algorithms implemented have allowed the use of comparatively low-cost devices in a demanding application. The road-edge detection system has achieved excellent results on curbed roads as well as extending the scope of such systems to roads without a clearly defined edge through tight integration of predictive filtering with the edge detection algorithm.

The user interfaces developed in this project have been tested and utilised extensively over the course of this year and have proven to provide powerful functionality as well as valuable tools for testing and refinement of the Autonomous SAE Car. The use of an asynchronous web-interface for robotics applications has been validated and it is evident that this technique has a strong future in the field. Safety has been actively considered throughout this project and the systems which have now been implemented provide mitigation of a wide variety of hazards in a manner which is robust, reliable and complements the operation of the vehicle.

The control systems implemented in this project have provided successful operation during testing and have seen the creation of a framework for control of the vehicle as well as improving understanding of the requirements for more advanced algorithms. The revised interpolating trajectory generation algorithm shows significant promise as the basis for more advanced methods and future work on this project will encompass optimisation of driving behaviours so that race grade performance can be achieved in the near future.

Future Work

There is significant scope for future work on this project now that the hardware and software platforms necessary for more advanced functionality have been developed and tested. The range of possible future projects involving the Autonomous SAE Car include improvements to sensor and communications systems, development of more advanced trajectory calculation and steering algorithms, further intelligent driving and mapping functionality as well as research into the operation of autonomous vehicles in traffic scenarios. The variety and scope of such work is substantial and should see the Autonomous SAE Car operated as a productive research tool for many years to come.

Potential improvements to the hardware platform would involve the integration of a better performing Wifi system, selection of a new GPS unit and the addition of image processing to the system. A communication system which would give reliable performance at distances up to 1 km and offer better immunity to interference would be extremely beneficial – in particular the new 800 MHz offerings from Ubiquity Networks [62] would be worth investigation. A more advanced GPS or GPS/INS combination unit such as the MTi-G-700 discussed in section 4.2 or, when available, an open source RTK solution such as the Piksi [63] would allow safer, more accurate, navigation and increase the flexibility of the vehicle. Image processing through the integration of a good quality video camera would also provide opportunities for greater functionality and research into the problem of fusing LIDAR and video data.

The development of optimised trajectory calculations with a greater level of pre-planning such that the “racing-line” is able to maximise speed and minimise distance over the course of the track would be extremely beneficial to this project. In addition to this, the steering and speed control algorithms could be improved through better characterisation of the dynamics of the Autonomous SAE Car to achieve performance at the limits of the vehicles abilities. An opportunity exists for the integration of dynamic map re-planning based on obstacle detection and ultimately the development of robotic driving algorithms which would operate without having a pre-defined map. In the foreseeable future this vehicle could be extended to navigate entirely based upon sensory inputs, with the goal of achieving total autonomy.

References

[1] SAE International. *"About Formula SAE Series"* [Online]. Available: http://students.sae.org/cds/formulaseries/about.htm. [Accessed: Oct. 20, 2013]

[2] T. Black. "A Driver Assistance System for a BMW X5." BE thesis, UWA, 2012.

[3] Siemens AG (2007). *"Tailored Solutions – Driverless Subways"* [Online]. Available: http://www.siemens.com/innovation/en/publikationen/publications_pof/pof_spring_2008/tailored_solutions/fahrerlose_ubahn.htm. [Accessed: Oct. 14, 2013]

[4] Rio Tinto Ltd. (2012, Feb.). *"Rio Tinto invests US$518 million in autonomous trains for Pilbara iron ore rail network in Western Australia"* [Online]. Available: http://www.riotinto.com.au/ENG/media/38_media_releases_1743.asp. [Accessed: Oct. 14, 2013]

[5] BBC (2013, Apr.). *"Robot truck platoons roll forward"* [Online]. Available: http://www.bbc.com/future/story/20130409-robot-truck-platoons-roll-forward. [Accessed: Oct. 14, 2013]

[6] Ernst D. Dickmanns. "The development of machine vision for road vehicles in the last decade", *Intelligent Vehicle Symposium*, pp. 268-281, 2002.

[7] S. Thrun, M. Montemerlo, H. Dahllamp et. al. "Stanley: The Robot That Won the DARPA Grand Challenge" in *The 2005 DARPA Grand Challenge*, M. Buelher, K. Iagnemma, S. Signh, Eds., Berlin: Springer, 2007, pp. 1-43.

[8] I. Miller, S. Lupashin, N. Zych et. al. "Cornell university's 2005 DARPA grand challenge entry", *Journal of Field Robotics*, vol. 23, no. 8, pp 625-652, Aug. 2006.

[9] M. Montemerlo, J. Becker, H. Dahikamp, D. Dolgov, S. Ettinger, D. Haehnel, T. Hilden, G. Hoffmann, B. Huhnke, D. Johnson, S. Klumpp, D. Langer, A. Levandowski, J. Levinson, J. Marcil, D. Orenstein, J. Paefgen, I. Penny, A. Petrovskaya, M. Pflueger. "Junior: The Stanford entry in the Urban Challenge", *Journal Of Field Robotics*, vol. 25, no. 9, pp. 569-597, 2008.

[10] J. Bohren, T. Foote, J. Keller et. al. "Little Ben: The Ben Franklin Racing Team's entry in the 2007 DARPA Urban Challenge", *Journal of Field Robotics*, vol. 25, no. 9, pp. 598-614, Sep. 2008.

[11] A. Bacha, C. Bauman, R. Faruque et. al. "Odin: Team VictorTango's entry in the DARPA Urban Challenge", *Journal of Field Robotics*, vol. 25, no. 8, pp. 467-492, Aug. 2008.

[12] A. Broggi, P. Medici, P. Zani, A. Coati, M. Panciroli. Autonomous vehicles control in the

VisLab Intercontinental Autonomous Challenge, *Annu. Reviews in Control*, vol. 36, no. 1, pp. 161-171, Apr. 2012.

[13] J. Markoff. "Google Cars Drive Themselves, in Traffic", *The New York Times*, Oct. 9, 2010 [Online]. Available: http://www.nytimes.com/2010/10/10/science/10google.html. [Accessed: Aug. 17, 2013]

[14] Electronic News Publishing. "Komatsu and Rio Tinto Enter into Agreement for 150 Autonomous Truck Deployment into Pilbara Iron Ore operations by 2015", *ENP Newswire*, 4 Nov. 2011.

[15] Komatsu Australia. *"Autonomous Haul System"* [Online]. Available: http://www.komatsu.com.au/AboutKomatsu/Technology/Pages/AHS.aspx [Accessed: Mar. 14, 2013]

[16] Adnan Shaout, Dominic Colella, S. Awad. "Advanced Driver Assistance Systems Past, Present and Future". *Seventh International Computer Engineering Conference*, pp. 72-82, 2011.

[17] Maximillian Muffert, David Pfeiffer, Uwe Franke. "A Stereo-Vision Based Object Tracking Approach at Roundabouts". *IEEE Intelligent Transport Systems Magazine*, Vol 5, Issue 2, pp. 22-32, Apr. 2013.

[18] Kirstin L.R. Talvala, Krisada Kritayakirana, J. Christian Gerdes. "Pushing the limits: From lanekeeping to autonomous racing", *Annu. Reviews in Control*, vol. 35, no. 1, pp. 137-148, Apr. 2011.

[19] Jan Seigemund, Uwe Franke, Wolfgang Forstner. "A temporal filter approach for detection and reconstruction of curbs and road surfaces based on Conditional Random Fields". *2011 IEEE Intelligent Vehicles Symposium*, pp 637-642, Jun. 2011.

[20] Vicente Milanés, David F. Llorca, Blas M. Vinagre, Carlos González, Miguel A. Sotelo. "Clavileño: Evolution of an Autonomous Car", *Annu. Conf. Intelligent Transportation Systems*, Madeira Island, Portugal, pp. 1129-1134, 2010.

[21] L. Brown. "Improving Performance Using Torque Vectoring on an Electric All-Wheel-Drive Formula SAE Race Car." BE thesis, UWA, 2013.

[22] T. Brown. "Handling at the limits", *GPS World*, vol. 21, no. 8, pp. 38-41, Aug. 2010.

[23] G. Gomez-Gil, S. Alonso-Garcia, F. J. Gomez-Gil, T. Stombaugh. "A Simple Method to Improve Autonomous GPS Positioning for Tractors", *Sensors*, vol. 11, no. 6, pp. 5630-5644,

May 2011.

[24] Wende Zhang. “LIDAR-Based Road and Road-Edge Detection”. *2010 IEEE Intelligent Vehicles Symposium*, pp 845-848, Jun. 2010.

[25] B. Fardi, U. Scheunert, H. Cramer, G. Wanielik. “Multi Model Detection and Parameter-based Tracking of Road Borders with a Laser Scanner”, *IEEE IV2003 Intelligent Vehicles Symposium,* pp. 95-99, Jun. 2003.

[26] W.S. Wijesoma, K. R. S. Kodagoda, Arjuna P. Balasuriya. “Road-Boundary Detection and Tracking Using Ladar Sensing”, *IEEE Transactions on Robotics and Automation*, vol. 20, no. 3, Jun. 2004.

[27] B. Dodson. (2012, Nov 11). “Autonomous Audi almost matches veteran race car drivers' lap times” [Online]. Available: http://www.gizmag.com/stanford-audi-tts-autonomous-car-thunderhill/24957/. [Accessed: Apr. 7, 2013].

[28] J. Eng. “Implementation of an Embedded System For Vehicle Avoidance For a BMW X5 System”, BE thesis, UWA, 2011.

[29] M. Himmelsbach, F. v. Hundelshausen, T. Luttel, M. Manz, A. Muller, S. Schneider, H.-J. Wunsche (2009). “Team MuCAR-3 at C-ELROB 2009”, *Proceedings of 1st Workshop on Field Robotics, Civilian European Land Robot Trial 2009* [Online] Available: http://www.ee.oulu.fi/research/robotics/celrob2009/workshop/papers/Team%20MuCAR-3.pdf. [Accessed: Jun. 30, 2013]

[30] National Coordination Office for Space-Based Positioning, Navigation and Timing (2013, Oct 16). *“GPS Accuracy”* [Online]. Available: http://www.gps.gov/systems/gps/performance/accuracy/. [Accessed: Jun. 24, 2013].

[31] USU/NASA Geospatial Extension Program (2010, Mar.). *“High-End DGPS and RTK systems”* [Online]. Available: http://extension.usu.edu/nasa/files/uploads/gtk-tuts/rtk_dgps.pdf. [Accessed: Sep. 3, 2013].

[32] Applanix (2010, Aug.). “*POS LV Position and Orientation System for Land Vehicles”* [Online]. Available: http://www.applanix.com/media/downloads/products/brochures/poslv_brochure.pdf. [Accessed: Apr. 5, 2013]

[33] QStarz. *“BT-Q818X User's Manual”* [Online]. Available:

http://www.qstarz.com/download/BT-Q818X-Users%20Manual.pdf. [Accessed: Sep. 3, 2013].

[34] D. Hennerström. “Increasing GPS Accuracy for Low Cost Receivers”, MSc Thesis, Luleå University of Technology, 2006.

[35] Xsens Technologies B.V. (2010, Oct.).*“MTi and MTx User Manual and Technical Documentation”* [Online]. Available: http://www.xsens.com/images/stories/products/manual_download/Mti_and_Mtx_User_Manual_and_Technical_Documentation.pdf. [Accessed: Mar. 6, 2013]

[36] T. C. Henderson, M. Dekhil, R. R. Kessler, M. L. Griss. “Sensor fusion” in *Control Problems in Robotics and Automation*, B. Sicilliano, K. P. Valavanis, Eds. Berlin: Springer, 1998, pp. 193-207.

[37] Marzullo, K. “Tolerating failures of continuous-valued sensors”, *ACM Transactions on Computer Systems*, vol. 8, no. 4, pp 284-304, 1990.

[38] W. Elmenreich. “Fusion of Continous-valued Sensor Measurements using Confidence-weighted Averaging”, *Journal of Vibration and Control*, vol. 13, no. 9-10, pp. 1303-1312, Sep. 2007.

[39] Xsens Technologies B.V. “*MTi-G-700 GPS/INS*” [Online]. Available: http://www.xsens.com/en/general/mti-g-100-series. [Accessed: Mar. 18, 2013]

[40] M. Abe. *Vehicle Handling Dynamics Theory and Application*. Burlington: Elsevier Science & Technology, 2009, pp. 5-7.

[41] G. Welch, G. Bishop (2006, Jul.). *“An Introduction to the Kalman Filter”* [Online]. Available: http://www.cs.unc.edu/~welch/media/pdf/kalman_intro.pdf. [Accessed: Oct. 2, 2013]

[42] O. Robescu. “Assessment of low-cost INS for positioning through sensor fusion with GPS”, MSc thesis, Chalmers University of Technology [Online]. Available: http://publications.lib.chalmers.se/records/fulltext/129978.pdf. [Accessed: Jun. 15, 2013]

[43] G. Falco, G. A. Einicke, J. T. Malos, F. Dovis. “Performance Analysis of Constrained Loosely Coupled GPS/INS Integration Solutions”, *Sensors*, vol. 12, no. 11, pp. 15983-16007, Nov. 2012.

[44] Yong Li, Jinling Wang, Chris Rizos, Peter Mumford, Weidong Ding. “Low-cost Tightly Coupled GPS/INS Integration Based on a Nonlinear Kalman Filtering Design”. *Proceedings of the 2006 National Technical Meeting of The Institute of Navigation*, Monterey, CA, pp. 958-966,

Jan. 2006.

[45] Honghui Qi, John B. Moore. “Direct Kalman filtering approach for GPS/INS integration”. *IEEE Transactions on Aerospace and Electronic Systems*, Vol 38, no. 2, pp. 687-693, Apr. 2002.

[46] ibeo Automotive Systems GmbH (2013, Sep.). *“IBEO Lux Datasheet”* [Online]. Available: http://www.ibeo-as.com/ibeo_lux.html. [Accessed: Sep. 30, 2013]

[47] National Imagery and Mapping Agency (2000, Jan.). *“Department of Defense World Geodetic System 1984”* [Online]. Available: http://earth-info.nga.mil/GandG/publications/tr8350.2/wgs84fin.pdf. [Accessed: May 15, 2013]

[48] W. Fraczek. “Mean Sea Level, GPS, and the Geoid”, *ArcUser* [Online], July-September 2003. Available: http://wou.edu/las/physci/taylor/g492/geoid.pdf. [Accessed: Oct 10, 2013]

[49] Geoscience Australia. *“Map Connect – 250K Topographic Map”* [Online]. Available: http://www.ga.gov.au/topographic-mapping/mapconnect.html. [Accessed: Oct 10, 2013]

[50] R. Rajamani. *Vehicle Dynamics and Control.* New York: Springer-Verlag, 2006, ch. 2.

[51] S. Haque. GENG2140 Lecture, Curve Fitting: “Spline Interpolation”. UWA, Semester 2, 2012.

[52] L. Poli. “User Interface for a Group of Mobile Robots” BE thesis, UWA, 2013.

[53] M.A. Goodrich, D.R. (Jr.) Olsen. “Seven principles of efficient human robot interaction”, *IEEE International Conference on Systems, Man and Cybernetics 2003*, vol. 4, pp. 3943-3948, Oct. 2003.

[54] J. Kock, M. Reichardt, K. Berns. “Universal Web Interfaces for Robot Control Frameworks”, *2008 IEEE/RSJ International Conference on Intelligent Robots and Systems*, pp. 2336-2341, Sep. 2008.

[55] D. Hazry, M. Sugisaka, T. Yuji. “Human-Robot Interface over the Web Based Intelligent System”, *American Journal of Applied Sciences,* vol. 3, pp. 1634-1639, Jan. 2006.

[56] S. Mootien, R. T. F. Ah King, H. C. S. Rughooputh. “A Web-Based Interface for the Gryphon Robot”, *2004 IEEE International Conference on Industrial Technology*, vol. 2, pp. 842-847, Dec. 2004.

[57] C. Paolini, G K. Lee. “A Web-Based User Interface for a Mobile Robotic System”, *2012 IEEE International Conference on IRI*, pp. 45-50, Aug. 2012.

[58] D. J. Smith, K. G. L. Simpson. *Safety Critical Systems Handbook.* Oxford: Elsevier Science,

2010.

[59] R. Woodman, A. F. T. Winfield, C. Harper, M. Fraser. “Building safer robots: Safety driven control”, *International Journal of Robotics Research,* vol. 31, no. 13, Nov. 2012.

[60] D. W. Seward, F.W. Margrave, I. Sommerville, G. Kotony. “Safe Systems for Mobile Robots – The Safe-SAM Project” in *Achievement and Assurance of Safety: Proceedings of the Third Safety-critical Systems Symposium*, F. Redmill, T. Andserson, Eds. London: Springer, 1995, pp. 153-170.

[61] Microchip Technology (2013, May). “*PIC16F87/88 Datasheet”* [Online]. Available: http://ww1.microchip.com/downloads/en/DeviceDoc/30487D.pdf. [Accessed: Sep. 17, 2013]

[62] Ubiquiti Networks. “*NanoStationM”* [Online]. Available: http://www.ubnt.com/airmax#nanostationm. [Accessed: Oct. 18, 2013]

[63] Swift Navigation Inc. “*Piksi: The RTK GPS Receiver”* [Online]. Available: http://www.kickstarter.com/projects/swiftnav/piksi-the-rtk-gps-receiver. [Accessed: Oct. 18, 2013]

Appendices

Appendix A – Acknowledgement of Software Licensors

The author would like to the thank the following people and projects for the use of their software libraries:

Author	*Library*	*License*
Adrian Boeing	KalmanPVA Class	1
ARM Limited	PID Library	MIT License
Boost Project	Boost C++ Libraries	Boost License
CodeCogs	linear.h (Linear Regression)	GNU GPL
gpsd Project	gpsd, gpsmm (GPS interface)	BSD License
Marcus Bannerman	Spline (From Dynamo Project)	GNU GPL
OpenCV Project	OpenCV (Kalman Filter)	BSD License
RGraph	RGraph (Javascript graphics)	Creative Commons Attribution
SharpDX Project	SharpDX (DirectInput interface)	MIT License
Terraneo Federico	AsyncSerial (Serial port API)	Boost License
Tim Black	IBEO Protocol Implementation	2

1. Freely available sample code not covered by a specific license.
2. Code and permission obtained from the author.

Appendix B – Drive-by-wire Command Set

This command set was developed in conjunction with Jordan Kalinowski for communication between the navigation controller and drive-by-wire controller.

Command	***Description***
S<X>	Set steering value to <X> in the range [-128,127].
A<X>	Set accelerator value to <X> in the range [0,255].
B<X>	Set brake value to <X> in the range [0,255]. Overrides A command.

Table 11: Drive-by-wire command set.

Error Code	***Description***	***Action***
ER0	Serial buffer overflow.	
ER1	Emergency brake engaged.	
ER2	WDT Timeout.	Trip
ER3	Brake servo on too long.	
ER4	Steering control fault.	Trip
ER5	No new command in 300ms.	Trip
ER6	Steering sensor out of bounds.	Trip

Table 12: Drive-by-wire error codes.

Appendix C – Base Emergency Stop Wiring Diagram

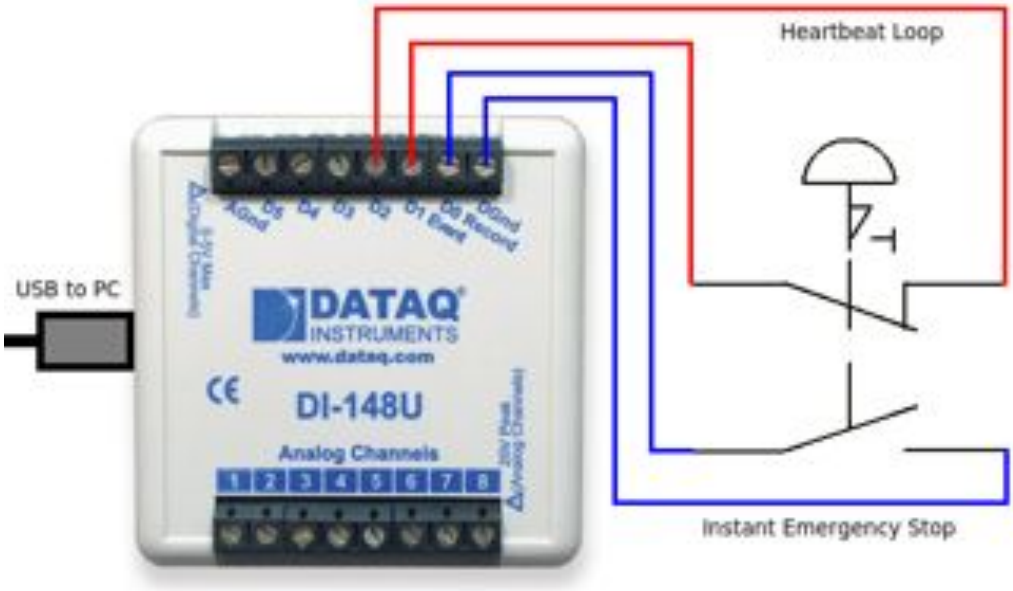

Appendix D – Web Interface

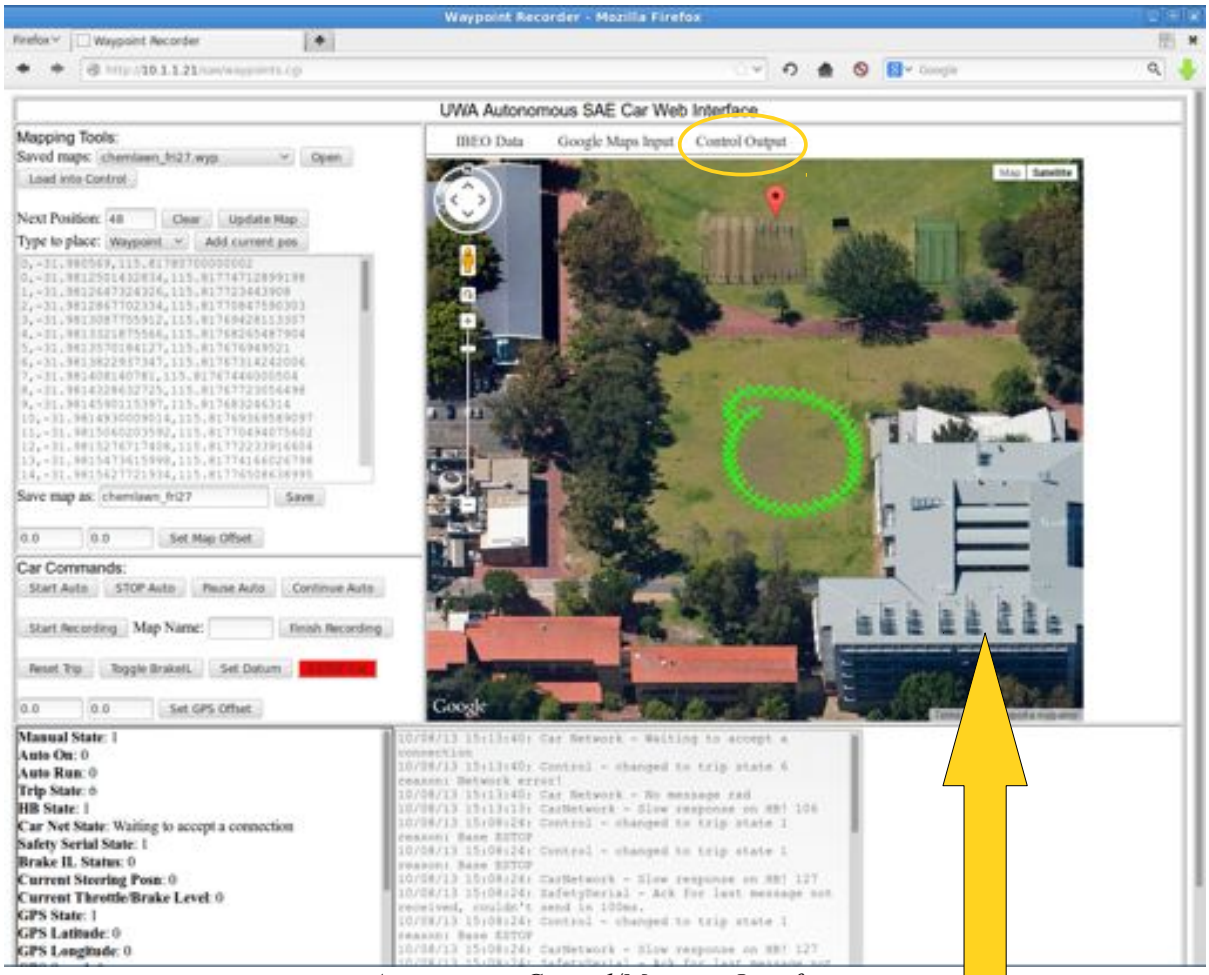

Autonomous Control/Mapping Interface

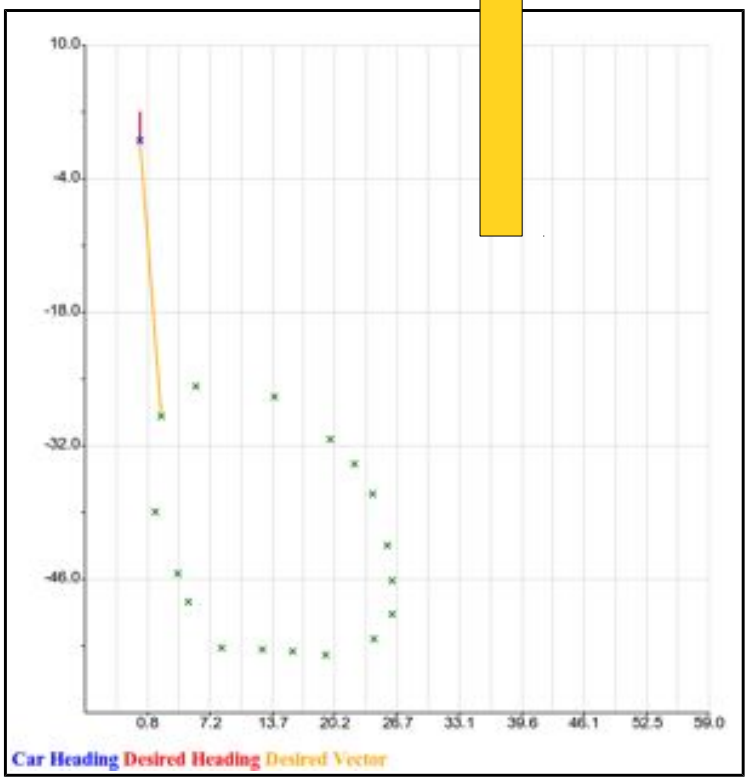

X-Y Control system output can be interchanged with Google Maps display.

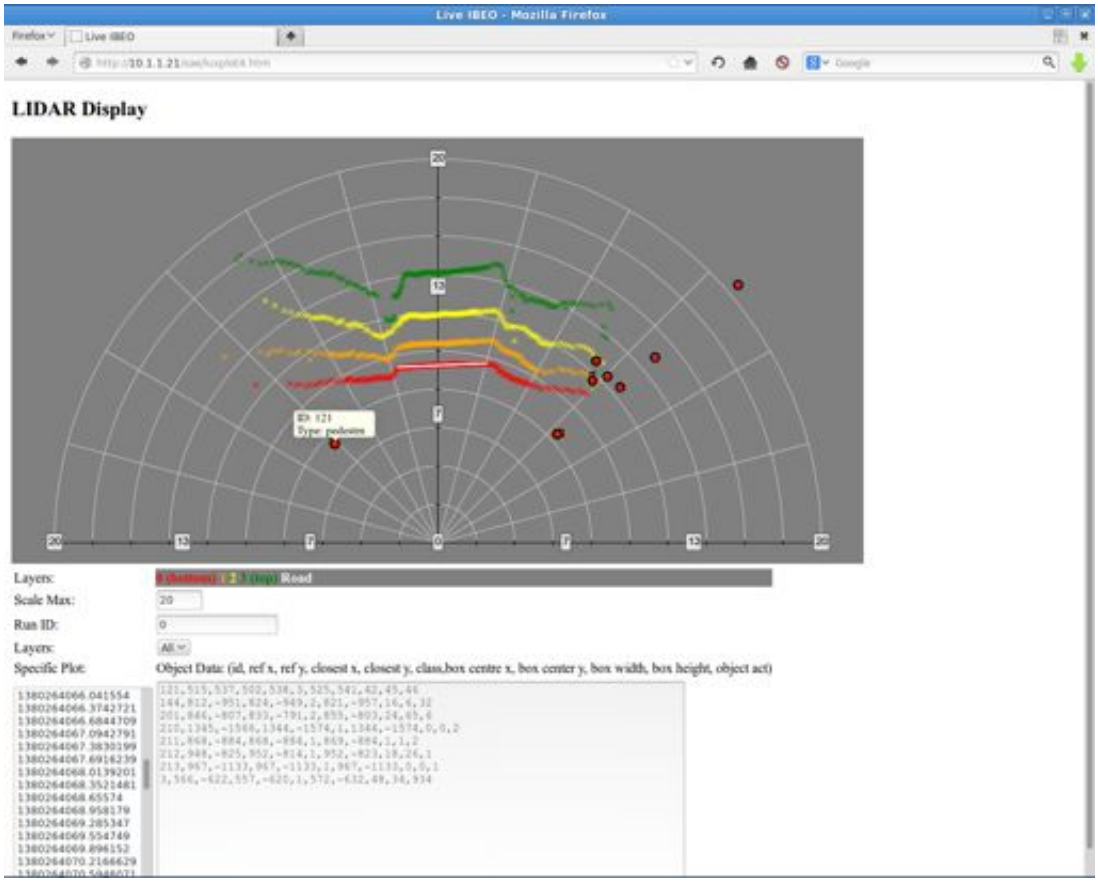

LIDAR Display Page

Risk No.	Risk	Risk - Likelihood Score (A)	Consequence Score (B)	Combined Risk Score (A) x (B)	Controls currently in place for this risk	Residual Risk - Likelihood Score (A)	Residual Risk - Consequence Score (B)	Combined Residual Risk Score (A) x (B)
1	Autonomous SAE car control failure – car travels outside designated area, possible person/property collision	5.00	3.00	15.00	- Pre-drive functionality testing - Appropriately sized area and restriction of driving course to central sections - Car to be run at extra low speed (<10 km/h) - Remote manual override - Remote emergency stop system - Loss of communication/control detection system - Automatic overrides for "safety driver". - Flashing warning light - Emergency alarm - Supervision by approx. 3 REV team members along perimeters during drive + 1 monitoring control system	2.00	3.00	6.00
2	SAE car (human driven) crash	2.00	3.00	6.00	- Driver PPE - Driver safety induction - Low speeds only (<20 km/h) - Course of sufficient size for stopping within perimeter - Driver emergency stop system - Flashing warning light - Supervision by approx. 4 REV team members along perimeters	1.00	2.00	2.00
3	Autonomous car unexpectedly accelerates from stationary during testing/setup	1.00	2.00	2.00	- Automatic safe arming sequence with throttle detection used when applying power to drive system	1.00	1.00	1.00
4	Inclement weather causes damage to car and/or base station	1.00	1.00	1.00	- Tent to be erected at edge of course or nearby safe area identified. - Monitoring of weather situation	1.00	0.00	0.00
5	Stationary car causes injury to person (electrical/mechanical hazards)	2.00	2.00	4.00	- Close supervision of cars - Appropriate covers/signage in place over wiring/mechanical parts	1.00	2.00	2.00
6	Electrical failure leads to fire or electric shock of driver	1.00	2.00	2.00	- Regular maintenance of vehicle including verification of electrical isolation.	1.00	2.00	2.00
7	Member of the public enters testing area and falls in path of vehicle	4.00	2.00	8.00	- Traffic cones and rope around the perimeter of the test area. - Supervision of perimeters	2.00	1.00	2.00
8	Inability to coordinate testing safely	2.00	1.00	1.00	- Manual remote or human driving as backup - Organisation of sufficient team members - Testing/practise sessions	1.00	1.00	1.00

RISK CONSEQUENCE SCORING

Consequence score	Financial	Media Coverage	Safety	Interruption to Research Activties
1	< $100k	Local Press (1 day)	No LTI	1 day
2	100 - 250k	Press (1 week)	LTI	2-7 days
3	250 - 500k	TV Local / State (Temporary)	Serious Injury	8-21 days
4	500 - 750k	TV Local / State (Extended)	Multiple Injuries	22 - 59 days
5	750k - 1m	Widespread National (Short)	Fatal	61 - 89 days
6	1m +	Widespread National (Extended)	Multiple Fatalities	90+ days

RISK LIKELIHOOD (% LIKELIHOOD) SCORING

	Chance of Occurring	Associated Score
Extra Rare	0 - 5 %	1
Rare	6 - 10 %	2
Unlikely	11 - 25 %	3
Possible	26 - 50 %	4
Probable	51 - 75 %	5
Almost Certain	75 - 100 %	6

Appendix F – Hardware Safety Supervisor Circuit

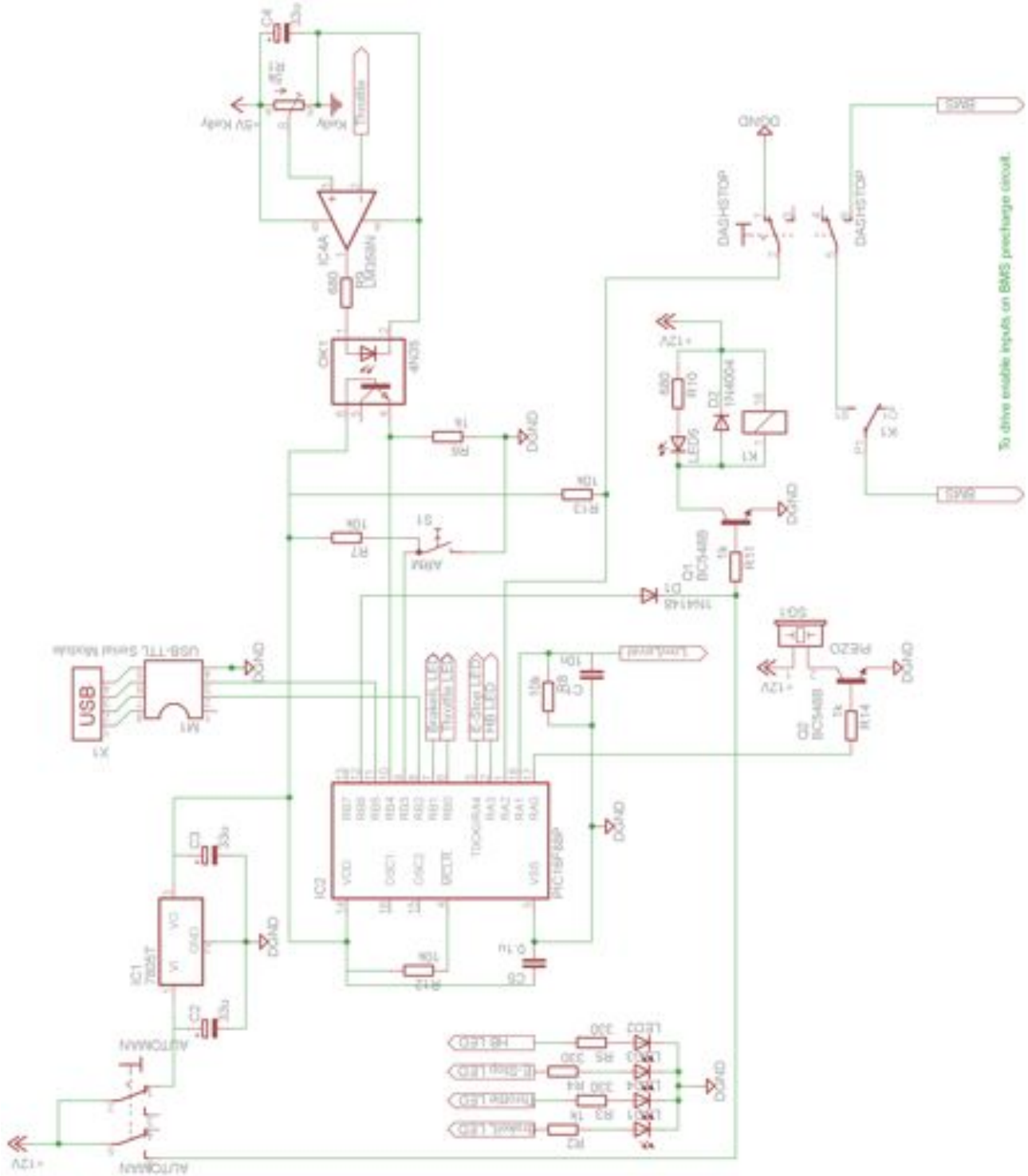

Appendix G – Safety Supervisor State Diagram

Appendix H – Safety Supervisor State Outputs

State	Output: Drive Enable Relay	Throttle LED	E-Stop LED	Piezo Alarm	Brake Interlock	HB LED	TX Message
RX Heartbeat						<HB>	ACK <HB>
Trip	0		1	1	1*	#	^TRIP
arm_state -1	0	%					AF <X>
arm_state 0	0	0	0	0	1*		AR
arm_state 1							A 1
arm_state 2	1						A 2
arm_state 3							A 3
arm_state 4							A 4
arm_state 5							A 5
arm_state 6					0		A 6
arm_state 7							A 7
arm_state 8							A 8
arm_state 9							A 9

Blank implies no change.

* When brakeil is enabled.
# 1 if HB was trip cause, else 0.
% 1 if throttle was the cause.
^ DES is sent first if the cause was the dash button or analogue driver safety module.
<HB> is the current hearbeat state.
<X> is 1 for arm button released, 2,3 for throttle sense.